2.8 Ga Subduction-related magmatism in the Youanmi Terrane and a revised geodynamic model for the Yilgarn Craton

Derek A. Wyman

School of Geosciences, The University of Sydney, NSW, 2006 Australia

derek.wyman@sydney.edu.au

Abstract

New studies in the central and southern parts of the Murchison Domain in the Youanmi Terrane, western Yilgarn Craton, reveal previously unidentified igneous rock types in addition to boninitic occurrences similar to those found in the northern part of the domain. New results also allow for a re-assessment of a volcanic suite previously described as examples of a "Karasjok type" of komatiite. The rocks are most plausibly examples of arc picrites, specifically of the type found in ophiolite settings. In addition to boninitic rocks and picrites, this study identified remobilized olivine-cumulate rich lavas that resemble examples found in the Troodos and Othris ophiolites. Examples of REE enriched high magnesium andesites exhibit pronounced high field strength element depletions on normalized plots combined with mantle-like Nb/Zr ratios. The rocks chemically resemble Phanerozoic examples of enriched boninites and their signatures are distinct from those typically attributed to crustal contamination of mantle plume magmas. Intrusions of the ~ 2792 Ma Warriedar Suite have compositions analogous to those of post-Archean Alaskan Intrusive complexes and were likely derived from subduction-modified sub-cratonic mantle. The new observations can be accounted for in a geodynamic scenario involving subduction along the western Yilgarn margin at ~ 2800 Ma. Similarities with the contemporaneous Superior Province raise the possibility that the nuclei of the two cratons were closely associated at this time.

Key words: Archean, arc picrite, boninite, Yilgarn, Youanmi Terrane

1. Introduction

The western Yilgarn Craton has historically received less attention than the well-known Eastern Goldfields, despite its distinct crustal architecture, isotopic characteristics and metal inventory (Champion and Cassidy, 2007). This imbalance has begun to change in recent years. Van Kranendonk et al. (2013) redefined the Archean stratigraphic sequence of the northern Murchison Domain and continued mapping efforts have extended this stratigraphy to the south (e.g., Zibra, 2015; Ivanic, 2018). Other studies of volcanic rocks include Wyman and Kerrich (2012), which described the geochemical characteristics of boninitic and other volcanic rocks and Lowrey et al. (2017) that reported on the first documented occurrence anywhere of platy pyroxene spinifex texture. Archean layered intrusive complexes, collectively the most voluminous in the world, occur in the Murchison Domain and were the subject of geochemical and isotopic studies by Nebel et al. (2103) and Ivanic et al. (2015). Granitic rocks and their sources have been discussed by Ivanic et al. (2012) and Ameen and Wilde (2018) and structural studies include those of Zibra et al. (2014).

The present study reports on Meso-Archean volcanic and shallow intrusive rocks from the southern part of the Murchison Domain of the Youanmi Terrane. It extends the known range of boninitic rocks in the Domain but also identifies other previously unknown rock types such as high-magnesium andesites and an Alaskan-style intrusive suite. The new results have important implications for the geodynamic evolution of the entire Yilgarn Craton because some of these rock types suggest a subduction-like process but are not readily explained by a mantle plume or by plume-induced crustal re-working, which is the most common scenario applied to the Meso-Archean Yilgarn in recent years (e.g., Van Kranendonk et al. 2013; Mole et al, 2014). We have also identified rocks that share compositional and textural features with a suite found in the Gabanintha area of the northern Murchison that Barley et al (2000) inferred were a variety of komatiite, based on apparent magma liquid compositions with > 22 wt% MgO. They named them “Karasjok-type”, which derives from a komatiite locality in Finnish Lapland in the Paleoproterozoic Karasjok greenstone belt (Barnes and Often 1990; Hanski et al. 2001). The key features of the Karasjok-type komatiites according to Barley et al (2000) are their volcaniclastic mode of eruption and similar Ti- and incompatible-element-rich, Al-depleted compositions. They inferred that the compositional features required interaction of deeply sourced mantle plumes with hydrated, subduction-modified and diamond-bearing lithosphere, a scenario that was not entirely consistent with most recent plume-only models applied to the Mesoarchean craton. The Karasjok classification appears to have been largely accepted and is included in Arndt and co-workers’ (2008) textbook on komatiites, despite the absence of olivine spinifex texture as acknowledged by Barley et al. (2000). The Gabanintha suite is re-assessed here based on a larger database for the suite and expanded knowledge of contemporary magmatism in the Murchison Domain; it is concluded they are not komatiites. In combination with the recognition of other subduction-style magmas, this reassessment of the Gabanintha suite requires a major revision to previous models, which commonly required the presence of a ~ 2.83 Ga mantle plume (Wyman and Kerrich, 2012; Van Kranendonk et al., 2013).

2. The Yilgarn Craton and Regional to Local Geology

The tectonic subdivisions of the Yilgarn have been revised and updated by numerous workers such as Czarnota et al. (2010), but the boundaries are increasingly considered to be mainly, or entirely, late features imposed upon a pre-existing craton (e.g., Smithies et al., 2018). The four main components are the Eastern Goldfields Superterrane (or Eastern Yilgarn Craton), the South-West terrane, the Narryer terrane and the Youanmi terrane. The latter is presently divided into the Southern Cross Domain in the east and the Murchison Domain in the west. The new Geological Survey of Western Australia (GSWA) lithostratigraphic framework for the Murchison Domain was first reported by Van Kranendonk and Ivanic (2009) and is based on regional mapping, geophysical data, remote sensing, and additional geochronological results. The structurally dismembered mafic-ultramafic layered intrusions in the northern and central Murchison Domain of the Youanmi Terrane are estimated to comprise approximately 40% by volume of the greenstones (Ivanic et al., 2000; 2015).

Four main volcano-sedimentary groups are recognized in the western Youanmi Terrane (Van Kranendonk and Ivanic 2009; Van Kranendonk et al. 2013; Ivanic, 2018). The occurrence of the 2960–2935Ma Mount Gibson Group in the south represents the most obvious difference compared to the northern Murchison Domain. Volcanic units in these older units in the Golden Grove and Mount Gibson areas are intermediate and felsic types intercalated with chemical sedimentary rocks and overlain by volcaniclastic mass-flow units and banded iron formation. Van Kranendonk et al. (2013) noted that there was a hiatus in magmatism between ~ 2930 Ma and 2830 Ma in the Murchison Domain (Fig. 2). The hiatus ended with deposition of the Singleton Formation of the Norie Group that includes the informal Gabanintha Suite (‘GA’) of Barley et al. (2000) and the Quinns Basalt Member that consists mainly of basaltic to andesitic Fe-rich tholeiitic rocks and smaller volumes of more evolved rock types. The Singleton Formation is overlain by felsic volcanic and volcaniclastic rocks and banded iron formation (BIF) of the Yaloginda Formation. Intercalated quartzite and BIF at the top of the formation are locally preserved. Given that the Yalgoginda Formation has been dated at about 2815 Ma to 2806 Ma (Van Kranendonk et al., 2013 and references therein), the Singleton Formation is likely to be all > 2815 Ma and is estimated to be up to 2825 Ma in age (Ivanic, 2018).

The Meekatharra Formation of the Polelle Group conformably overlies the Norie Group and consists of tholeiitic basalts, pyroxene spinifex-textured Siliceous High Magnesium Basalts (SHMB) and boninites, locally inter-bedded with minor felsic volcanic and volcaniclastic units (Wyman and Kerrich, 2012; Lowrey et al., 2017). A 2799 +/-2Ma rhyolite volcaniclastic in the Polelle Syncline, is interpreted to be the end of the Norie and start of Polelle and a dolerite sill in the underlying Norie Group, which may be a feeder to Polelle mafic magmas, has an age of 2792 ± 5 (Van Kranendonk and Ivanic, 2009). The conformably overlying Greensleeves Formation consists of andesitic to rhyolitic volcanic and volcaniclastic rocks and is in turn conformably overlain by BIF and felsic volcaniclastic rocks of the Wilgie Mia Formation. The overlying c. 2735 - 2700 Ma Glen Group includes coarse clastic and finer grained felsic volcaniclastic rocks. A thick lower unit of pyroxene spinifex-textured basalt and pillowed basalt, locally interbedded with andesitic to rhyolitic volcanic rocks, conformably overlies these sedimentary units, or overlies rocks of the Greensleeves Formation (Van Kranendonk et al 2013).

A notable feature of the western Yilgarn Craton, and the Murchison Domain specifically, is the presence of an isotopically juvenile crustal zone defined on the basis of granitoid whole rock Sm-Nd compositions, originally documented by Champion and Cassidy 2007 (Fig 1b). The distribution of relatively juvenile crust corresponds closely to that of greenstone belts and layered intrusions.

The Singleton Formation is well exposed at Mt. Singleton where a local stratigraphic succession was established in detail (Lipple et al., 1983; Ivanic, 2018; Fig. 3a). The Singleton syncline has a shallow plunge of 5- 10 degrees near Mt Singleton. Dips are moderate to steep and way up directions are defined by mafic pillows, flow tops, grading within intrusions, and sedimentary features. A U-Pb zircon age of 2805 ± 5 Ma from near the top of Mt Singleton, corresponding to the “agglomerate” of Lipple et al. (1983; Fig. 3a), is interpreted as a maximum depositional age for that unit (Wingate et al., 2013).

The geology of the Mt Magnet area has most recently been summarised by Zibra (2015). Sampling in this study focussed on the Singleton Formation employing drill core from the Saturn Pit in the Galaxy Mining area of Ramelius Resources Ltd, previously described by Thompson et al. (1990), and samples collected at surface in the area (Fig. 3b). The stratigraphy in the Saturn Pit area is dominated by mafic flows and iron formation with lesser intercalated felsic tuffs and carbonate-altered ultramafic units. Thompson et al. (1990) interpreted these as flows but they also include shallow-level intrusive bodies.

3 Results

Analytical techniques and previously unpublished whole rock major and trace element data are given in Supplementary File 1 and Table S1. A variety of texturally distinct volcanic rock types occur at the Mt. Magnet and Mt. Singleton localities and include fragmental volcaniclastic and hyaloclastic units, pillowed, variolitic and massive mafic to ultramafic lava flows and tubes, with and without acicular or spinifex pyroxene textures in mafic to intermediate rocks as described below (Fig. 4). Various mafic to ultramafic intrusions ranging up to 100's of meters in thickness are noted in published descriptions by Lipple et al. (1983), Thompson et al. (1990), and others. Metamorphic grade is generally greenschist facies, meaning that preservation of primary mineral phases does not correspond to the exceptional levels observed locally in the northern Murchison (Wyman and Kerrich, 2012; Lowrey et al., 2017). Nonetheless, textural details are commonly well-preserved and occasional relict primary minerals are observed.

3.1 Geochemical Results

New whole rock data for samples from the Mt Magnet (MM) and Mount Singleton (MS) areas are compared with those of the "Karasjok-type" suite and associated volcanic units in the Gabanintha area (collectively referred to here as "GA"). Data in Table S1 are reported as presently in the WACHEM database or not yet included in WACHEM at the time of writing. In some cases, data from the larger GSWA Murchison geochemical database of volcanic rocks (WACHEM, 2018) are also plotted for comparison (Fig. 9, 10A, 12A). The plots include shallow-level intrusive samples that can be correlated with volcanic rock types within the MM and MS sections or elsewhere in the southern Murchison, as described below.

3.1.1 Major Elements

Harker diagrams are given in Figure 5. The trend to the upper left of the MgO plot (higher MgO at lower SiO_2) suggests that accumulation of olivine may have occurred in samples with MgO greater than about 16 wt% MgO. The diagrams also highlight MM and MS subsets marked by high TiO_2 (> 1.5 wt%) and P_2O_5 (> 0.24 wt %), which do not fall on the respective main trends defined by the majority of samples and suggest a distinct magma evolutionary path. They correspond to samples with relatively high SiO_2 (50 to 60 wt%), rather than in mafic-ultramafic samples, and represent the Quinns Basalt member discussed below or shallow gabbroic intrusions (see also Fig. 9).

A plot of Al_2O_3/TiO_2 versus TiO_2 and Al_2O_3 is shown in Figure 6a and 6b. The curve defined by maximum TiO_2 contents at any Al_2O_3/TiO_2 value represents a common fractionation feature similar to those of many greenstone belt sequences (e.g., Wyman and Hollings, 2006). At least 2 sub-trends can be identified extending to lower TiO_2 contents away from the main trend. In general, the further these samples plot off of this trend, the higher their MgO content, consistent with accumulation of olivine and pyroxenes and the "dilution" of TiO_2. The trend at Al_2O_3/TiO_2 ~ 15 to 18 mainly includes many (S)HMB samples from MM. The trend at Al_2O_3/TiO_2 = 11 to 8 includes the Gabanintha "Karaskjok-type" samples given by Barley et al. (2000), similar rocks from the same area reported by Wyman and Kerrich (2012) and MS samples with similar trace element attributes (e.g., normalised plots: Fig.s 9i, 10b). These rocks are Al-depleted and many have Al_2O_3 contents between 7 and 4 wt%. Most of the MM samples in this low Al_2O_3/TiO_2 trend are examples of later (c. 2790) Alaskan-type intrusions (typically with $Al_2O_3 \approx 10$ wt%) not found in the Gabanintha area but which have important trace element features as discussed in the following section.

3.1.2 Trace Elements

Whole rock Th, Nb and Zr abundances are shown on x-y plots in Figure 7 and highlight multiple trends in the more evolved rocks of each area. These are most readily distinguished on the Zr vs Th plot (Fig 7b) where the highly incompatible elements define five trends and provide an indication of the minimum number of magma systems represented by the studied samples. The U vs Th plot shows that the two elements co-vary in most suites, except for a small number of high-Th samples from Mt Magnet (Fig. 7d).

No REE x-y plot provides arrays that correspond to the multiple trends on the Zr vs Th plot, likely because some of the magma suites have similar initial REE abundances and distributions and because the range of compatibilities of the light to heavy REE during magma evolution does not preserve REE x/y ratios. Nonetheless, it is evident that the MS samples overlap the mafic-ultramafic members of the GA suite whereas the MM samples also overlap but extend to much higher La/Sm ratios that are accompanied by systematically lower Zr/Zr* values (Fig. 8), where Zr* is derived from the primitive mantle normalized abundance given by: $(Nd_{PM})^{0.5} \times (Sm_{PM})^{0.5}$.

3.2 Mount Magnet

Normalized multi-element plots help to distinguish the various magmatic sub-groups and illustrate the chemostratigraphy of the two study areas (Fig. 9). Samples from MM drill core are described in their inferred stratigraphic order. Samples collected to the east of the mine occur in the Singleton Formation or represent the overlying Yaloginda Formation, based Geological Survey of Western Australia mapping of the district (Zibra, 2015). A group of drill hole samples from small intrusions are correlated with the ~ 2792 Ma Warriedar intrusive suite, based on their abundant coarse amphibole content (Fig.s 4e; 9d).

The deepest sample in the sequence is a boninitic high-Mg andesite (GX10-530) that has 53 wt% SiO_2, 8.1 wt% MgO, 0.41 wt% TiO_2 and an Al_2O_3/TiO_2 ratio of 41. Normalized plots (Fig. 9) display a concave upward pattern for the REE's and minor negative Eu and Ti anomalies in some samples combined with a prominent Nb trough and a high Th/Nb ratio (Fig. 9c). Although sampled only once in drill core, similar rocks were sampled in the Mount Magnet area and are also shown in Figure 9c.

The overlying unit consists of variably carbonate- and sulphide-altered basaltic andesite flows (LOI = 3 – 11 wt%) with Au mineralization-related carbonate and pyrite ± sericite, as shown in drill logs and assays of Ramelius Resources Ltd. Based on their similarity to previously published data (Watkins and Hickman, 1990), these rocks are tentatively assigned to the Quinns Basalt unit, which now has Member status within the Singleton Formation. Their major element contents (recalculated volatile-free), however, are relatively uniform with ~ 51 - 53% wt SiO_2, ~ 17 wt% Fe_2O_3, 5 to 6 wt% MgO, 2.2 wt% TiO_2 and low Al_2O_3/TiO_2 ratios of 5.5 to 6. Their multi-element patterns are consistently flat, with only minor Nb troughs, slight negative Ti anomalies and no Th enrichment (Fig. 9b). A few samples display very minor positive Zr-Hf anomalies that could be a primary feature of the liquid, or may reflect REE loss. The patterns consistently display high HREE/Al and high V/Sc ratios that preclude significant magnetite fractionation. Typical Zr/Y ratios are ~ 3. Archean and Proterozoic examples of these rock types are relatively common in both mantle plume and subduction-related environments and have previously been described as Icelandites or Icelanditic (e.g., Wyman et al., 1999; Gibson et al., 2007), although the type examples are now recognized as "Fe-Ti rich tholeiitic andesites" (Sigmarsson and Steinthórsson, 2007). They are ascribed to near-solidus fractionation of tholeiitic magmas and (or) remelting of tholeiitic mafic crust (Jonasson, 2005; Kuritani et al., 2011). The basaltic andesite sequence contains an intercalated, highly carbonate-altered interval (Sample GX12-471; LOI = 12.8 wt%) that appears to be an example of the overlying sequence of rocks, although it may be a sill.

The Fe-Ti rich tholeiitic basaltic andesites are overlain by volcanic rocks that display a wide range of SiO_2 and MgO contents but exhibit consistent trace element signatures (Fig. 9a). Ultramafic examples (MgO = 20 to 31.5 wt %) immediately overlie the second volcanic suite in one drill hole. They have SiO_2 between 46 and 48 wt%, TiO_2 between 0.4 and 0.6 wt%. Although they broadly resemble the GA suite (Fig. 10) on normalized plots, their Al_2O_3/TiO_2 ratios (mainly ~ 16) are higher than the Gabanintha occurrences. Their normalized patterns exhibit moderate LREE enrichment ($[La/Yb]_{CN}$ = 1.6 to 2.5) and slightly fractionated MREE-HREE ($[Gd/Yb]_{CN}$ = 1.2 – 1.5). These rocks transition upward to lower Mg counterparts (MgO ~ 10 wt %) that are free of an obvious mineralization-related metasomatic overprint but have similar trace element patterns. In some cases, the rocks contain cm-scale amphibole (partially chloritized), possibly after acicular pyroxenes. Although the trace element patterns are similar in terms of deep Nb anomalies and normalised REE abundances that increase toward the LREE, the presence of minor positive Zr-Hf anomalies in some samples may again be an artefact of alteration-induced REE loss. For example, the anomalies are not present in the least altered samples (e.g., MMD 12-182 vs MMD 12-204B) and small negative anomalies occur in other samples. The $[Th/U]_{PM}$ ratios remain quite consistent at ~ 1 over a wide range of Mg contents.

Small intrusions are abundant at the Mount Magnet deposit in the Hill 50 area and those sampled in core are amphibole rich, commonly ~ 75% coarse euhedral amphibole that has been variably overprinted by carbonate minerals. Chemically, they share some features with volcanic rocks in the immediate Mt Magnet area (e.g., the Hy Brazil farmstead occurrences), such as distinct Nb (Ta) and Zr-Hf depletions combined with moderate REE fractionation and LREE enrichment. In detail, however, they most closely resemble gabbros in the Warriedar area (WR 17 in Fig 9d) and therefore are assigned here to the ~2792 Ma Warriedar suite (Ivanic, 2018). The combination of low Al_2O_3/TiO_2 ratios (10-12), enriched LREE, prominent Zr-Hf negative anomalies and high $[La/Nb]_{PM}$ combined with much lower $[Th/Nb]_{PM}$ ratios are relatively uncommon in Archean greenstone belts but their normalized patterns very closely resemble Paleoproterozoic examples of Alaskan intrusive suites from the North China Craton (Yuan et al., 2010) and the Alaskan suites themselves. The latter include hornblendites among a wide range of rock types in fully developed post-Archean complexes derived from hydrous saturated basaltic magmas (Himmelberg and Loney, 1995). Alaskan complex rock types that match the MM suite in terms of SiO_2 and MgO contents also display similar Al_2O_3/TiO_2 ratios.

Outside of the Saturn Pit and to the east, several rock types were identified. These include Norie Group rocks that resemble the northern Murchison Domain Siliceous High Magnesium Basalts (SHMB) of the Polelle Group discussed by Lowrey et al. (2017). The SHMB (Fig. 9f) typically have SiO_2 contents of 53-54 wt% combined with MgO of 10 – 14 wt%, TiO_2 between 0.6 and 1.0 wt%, and

Fe_2O_3 and Al_2O both mainly ~ 11 wt%. Their LREE are slightly enriched with $[La/Sm]_{CN}$ generally between 1.5 and 2.0 and the HREE are slightly depleted in most samples ($[Gd/Yb]_{CN}$ = 1.2 – 2.0). Minor normalized Zr-Hf depletions relative REE are usually present (Zr/Zr* ~ 0.8) but Nb troughs are more pronounced (Nb/Nb* ~ 0.3 – 0.5). Slightly more evolved rocks are also assigned to the Singleton Formation by Zibra (2015), which in this area was termed the Murrouli Basalt prior to revision of stratigraphic nomenclature. Samples of these rocks have higher SiO_2 contents (53 – 58 wt%) and Al_2O_3 (~ 14.5 wt%) but lower MgO (4 – 6.5 wt%) and Fe_2O_3 (6.7 – 11.3 wt%). Their LREE are more enriched than in the SHMB ($[La/Sm]_{CN}$ = 2.3 – 4.5) and the HREE display less relative depletion ($[Gd/Yb]_{CN}$ = 1.2 – 1.5). Both the SHMB and the more evolved samples are locally carbonate-altered but secondary amphiboles faithfully pseudomorph pyroxene, including zoning in acicular spinifex pyroxenes and common cruciform textures.

Other rocks east of Mt. Magnet occur in a map unit that consists of metamorphosed mafic to ultramafic volcanic flows and cumulates (Zibra, 2015). They have not been assigned a place within the stratigraphic sequence but are intruded by a gabbro of the ~ 2792 Ma Warriedar suite. These rocks are tentatively assigned to the Yalgoginda Formation based on the fact that the most compositionally distinct examples lack coarse spinifex or acicular textures and are only weakly porphyritic and amygdular. These rocks are unlike any others previously reported in the Murchison Domain. In order to distinguish them from the previously described Singleton Formation examples and based on typical SiO_2 of ~ 56 and MgO contents of mainly ~8 wt% (one sample has 11 wt%), respectively, they are collectively referred to here as High-Magnesium Andesites (HMA). They have low TiO_2 contents (generally < 0.4 wt%) and high Al_2O_3/TiO_2 ratios. Their normalized trace element patterns exhibit pronounced REE fractionation, mainly from relative LREE enrichment. They display more pronounced Nb and Zr-Hf anomalies than other MM rock types and some have high $[Th/Nb]_{PM}$ ratios that correspond to the off-trend samples on the U vs Th plot of Figure 7d and extend the correlation of $[La/Sm]_{CN}$ to low Zr/Zr* values in Figure 8b. The rocks resemble the “enriched boninites” associated with rifting of the northern Tonga Ridge (Falloon et al., 2007). Both suites have Zr/Y ratios near mantle values but the MM rocks display stronger REE enrichments relative to the HFSE.

3.3 Mount Singleton

The MS volcanic samples all belong to the Singleton Formation, which is more fully developed than in the Mt. Magnet Saturn Pit area (Fig. 9), but does not include any examples of the Quinns Basalt Member, which is not exposed here. Boninitic signatures occur in the lowermost MS samples (TiO_2 < 0.20 wt%; Al_2O_3/TiO_2 25 – 33). They are distinguished by low overall incompatible element contents (mainly ≈ primitive mantle) and concave-up normalized multi-element patterns. They are a petrographically distinctive suite of cumulate-rich rocks (MgO ~ 36 wt%) where even the walls of lava tubes or magma conduits contain abundant olivine phenocrysts. Analogous rocks are relatively rare in the geological record but compositionally and texturally similar occurrences are known from the Upper Pillow Lavas from the Margi area of the Troodos ophiolite (Taylor, 1990; Bailey et al., 1991). A sample of the Margi picritic unit is plotted for comparison (Fig 9j).

Above these olivine cumulate flows, a suite of mafic differentiated flows (Mg0 = 5 to 16 wt%) share common normalised patterns. Those with the highest MgO contents have Al_2O_3 of ~ 5 wt% and TiO_2 contents of ~ 0.6 wt%. Key features of their multi-element patterns closely match those of the GA suite. They have similar Al-V-Sc patterns and slightly rising REE patterns with $[La/Sm]_{CN}$ mainly ~ 1.2 and $[Gd/Yb]_{CN}$ mainly 1.3 to 1.8. As a group, they also display minor Zr-Hf depletions versus the MREE, as is the case for the Gabanintha mafic to ultramafic rocks. Both suites also display moderate Nb depletions versus La and Th and primitive mantle normalised Th/U generally less than 1.

Thin ultramafic agglomerates occur within the basalts (MgO = 23-26 wt%). These have relatively flat normalised patterns but slightly humped REE ($[La/Sm]_{CN}$ ≈ 0.60 – 0.75; $[Gd/Yb]_{CN}$ ≈ 1.47 -1.64). Basalts and gabbros higher in the sequence tend to display less MREE/HREE fractionation and basalts have progressively less V enrichment versus Al or Sc. The multi-element patterns of the uppermost flows, tuffs and agglomerates also lack pronounced positive V anomalies and some of the upper basaltic rocks have $[Gd/Yb]_{PM} < 1$ and weakly concave upward REE patterns. Although the rocks have SiO_2 contents of 51 to 53 wt% and MgO contents of about 8 wt%, their TiO_2 contents of ~ 0.59 wt% places them slightly outside of the boninites field on discrimination diagrams (e.g., Cooper et al., 2010).

4 . Discussion

4.1 Crustal Contamination

Given the isotopic evidence for older crust recognized in the western Yilgarn (Cassidy et al., 2006; Champion and Huston,2016), the possibility that particular MM, MS or Ga volcanic suites may be hybrid products generated by crustal contamination of mantle magmas must be considered. A regional-scale isotopic study for the southern Murchison is presently underway and results will be compared to those of Wyman and Kerrich (2012) and papers in preparation for the northern Murchison. For the present study, the objective is only to establish that crustal contamination was not severe in the MM and MS sample sets and was not responsible for the development of any of the main volcanic suites.

It is clear that the MM examples of the Quinn's Basalt tholeiitic suite (Fig. 9B) cannot have been strongly modified by a crustal component. They display very low primitive mantle normalized Th/Nb and Th/La ratios, lack Ti or Eu anomalies and have flat multi-element patterns that preclude a significant contribution from evolved crustal sources. Similarly, the olivine-phyric boninitic flows display Th/Nb ratios comparable to those of their Troodos counterpart from the Margi area (Fig. 9I), despite being the most likely of all MM and MS rock types to have been modified by crustal assimilation in a crustal magma chamber. They also display low MREE/HREE ratios that do not permit whole-sale assimilation of shallow crust. Wyman and Kerrich (2012) reported isotopic data for an extremely well preserved boninite, with classic acicular pyroxene texture, from the northern Murchison Domain that falls within the range of the boninites reported here. Its $\varepsilon Nd_{2800\ Ma}$ of -1.6 might be interpreted as indicative of crustal contamination but would also be consistent with a petrogenetic scenario involving a subduction setting. For comparison, Lesher and Arndt (1995) considered the Paringa basalts of the Kambalda area to be highly contaminated komatiites and they also have εNd_T of about -1.2 to -2.4. Their trace element compositions as summarised on mantle-normalised plots feature high normalised LREE/MREE ratios that Said and Kerrich (2009) argued showed no correlation with εNd_T, implying these were all features of a heterogeneous source. Irrespective of that debate, the trace element features of the Paringa basalts illustrate how different a boninite and contaminated komatiite signature are likely to be, based on commonly applied crustal assimilation models (Lesher and Arndt, 1995; Mole et al, 2018). Some tholeiitic Norie Group flows near Cue (north of Mt Magnet) exhibit stronger incompatible element depletion than seen in the boninites (Wyman and Kerrich, 2012). They might be considered to represent potential parental magmas in a contamination scenario. However, they lack the positive Zr/Zr*observed in the boninitic rocks and so this feature would need to be attributed to the contaminant. The positive Zr-Hf anomalies in boninites are generally ascribed to slab melt metasomatism in boninites (e.g., Woelki et al., 2018 and references therein) but no potential Yilgarn crustal component can generate such positive anomalies via contamination of the Cue depleted basalts and match other features of the boninites. For example, the Cue rocks have Th-Nb-La relative abundances that are similar to those of the boninites but their MgO contents (6-9 wt% MgO: Wyman and Kerrich, 2012) are lower than the boninites. Conversely, the association of depleted basalts and boninites in the Murchison Domain is readily accounted for without a crustal contamination scenario, given their common association in Phanerozoic settings.

Barley et al. (2000) considered the possibility of crustal contamination in the formation of Gabanintha suite. They noted that normalized Nb depletions occurred in the suite but argued that any shallow level contaminant of ultramafic samples would require relatively low SiO_2 contents combined with Al_2O_3/TiO_2 much less than 20 in order to generate the characteristic features of the suite from contamination of either “Al-depleted” or “Al-undepleted” komatiites. On this basis, they ruled out continental contamination and advocated a scenario involving mantle plume ascent beneath subduction-modified continental margin lithosphere. It will be argued below that the parental magma liquid compositions of the Gabanintha “Karasjok” suite were actually close to 16 wt% MgO, but the Barley et al (2000) arguments against crustal contamination in a “plume only” scenario remain applicable. Wyman and Kerrich (2012) reported Sm-Nd isotopic data for four Norrie Group samples from the Gabanintha area (MgO = 14.4 to 2.5 wt % with corresponding εNd_{2800Ma} = 0.9 to -0.5) where the highest-MgO sample had εNd_{2800Ma} = 0.3 along with $[La/Yb]_{CN}$ = 2.6 and Nb/Nb* = 0.54 (Nb* extrapolated from mantle-normalized Th and La). On this evidence, we also conclude that the variable incompatible enrichment observed in the Gabanintha ultramafic rocks (e.g., $[La/Sm]_{CN}$ typically 0.8 to 1.0 in cumulate-rich rocks but 1.3 – 1.7 at MgO ~ 16 wt%) must be sub-crustal in origin.

The multi-element signatures of Alaskan intrusion-style MM samples display negative Zr anomalies versus the MREE and low enrichments of Th versus Nb and LREE that are typical of these intrusive suites through the Proterozoic and Phanerozoic (Himmleberg and Loney, 1995; Wang et al., 2010). In addition, contamination-sensitive trace element ratios for these rocks and most other MM and MS suites do not evolve with indices of fractionation. The MM East HMA surface samples (Fig. 9e) also display very strong Zr-Hf troughs and MREE-LREE enrichments. They are distinguished from the Alaskan suite by high but variable Th/Nb ratios and lower Zr/Y ratios (Fig. 9d). Notably, their relative Nb-Ta-Zr-Hf abundances are similar to those of magmas derived from depleted mantle sources. This combination of features cannot reasonably be accounted for by contamination of non-arc mantle magmas with evolved Murchison crust. They are distinct from Yilgarn lithologies that may plausibly have been derived via crustal contamination, which have high Zr/Y and lack the mantle-normalised Zr-Hf depletions, because the proposed TTG crustal contaminant does not possess this feature (e.g., Said and Kerrich, 2010; Barnes and Van Kranendonk, 2014). In post-Archean subduction-related rocks, the presence of Zr-Hf depletions is generally attributed to sediment melting under conditions where residual zircon remains behind (Elliott et al., 1997; Hermann and Rubatto, 2009). It is worth noting that Archean diamond-bearing lamprophyric shoshonite diatremes of the southern Superior Province display similar trace element patterns, SiO_2 and MgO contents and the low Al_2O_3/TiO_2 ratios of the Saturn pit amphibole-rich gabbros and Alaskan suites. Both the “late tectonic” Alaskan suite and the lamprophyres are ascribed to melting of subduction-metasomatised lithospheric mantle (Yuan et al., 2017; Wyman et al., 2008).

The geochemical and isotopic compositions of the contemporaneous (c. 2800 Ma) Narndee Igneous Complex, located between Mt Magnet and Mt Singleton are also relevant. Most units in the complex display low Nb/Nb* (typically 0.2 to 0.4) and negative normalized Zr-MREE anomalies as observed in several MM and MS rock types and commonly found in subduction-related magmas (Hirai et al., 2018). These anomalies are combined with low mantle-normalized Th/La ratios, generally less than one (as in the original "Alaskan" suite), and moderate LREE enrichment, most commonly with $[La/Yb]_{CN}$ between 1.2 and 2.5 (WACHEM, 2018). Ivanic et al. (2015) showed that the zircon Hf, whole-rock Hf and Nd isotopes, along with H and O isotopes amphibole and O isotopes in zircon from the complex, indicated only very minor crustal contamination and a mantle origin for the HFSE-REE features found in the complex and probably other ~2800 Ma rocks of this study. The multi-element pattern of the Narndee Igneous Complex gabbro from which Ivanic et al. (2015) obtained their mantle-like zircon εHf results is shown in Figure 9a and it resembles the patterns of many samples included in this study.

4.2 Wet Magmas

As noted by Falloon et al. (2000, p. 698), Phanerozoic "boninites are an important 'end-member' supra-subduction zone magmatic suite as they have the highest H_2O contents and require the most refractory of mantle wedge sources" and it is generally accepted that boninite major element compositions require an origin in the shallow mantle and a contribution from a water-rich fluid (Reagan et al, 2010). Although inferences concerning the geodynamic significance of Archean boninites based on much younger occurrences must be made with care, petrologic considerations imply that the Archean examples were also likely derived from "wet" magmas. For example, depletion of the MREE versus the HREE, combined with LREE enrichment and concave normalized REE patterns, establishes similar requirements for source depletion and re-enrichment for young and old boninites, as does the common suppression of feldspar phenocryst formation and the high-Mg nature of the magmas (Taylor et al., 1994). Based on younger boninites examples, the variable development of positive Zr-Hf anomalies versus the MREE does, however, suggest a contribution from melts to their source as previously noted (e.g., Woelki et al., 2018). Pearce and Robinson (2010) summarise the findings of numerous studies (e.g., Langmuir et al., 2006; Portnyagin et al., 1997) for a wide range of mantle potential temperatures (Tp) associated with Phanerozoic boninites localities, including Tp ≥ 1400° C. As is the case for some Archean boninites (Abitibi belt: Wyman and Kerrich, 2009), the higher Tp values may in some instances have been associated with mantle plume material, although Pearce and Robinson (2010) favour a slab edge mantle flow model to account for the Tp ~ 1400° C associated with the Troodos Lower Lavas. Estimates of Archean ambient upper mantle Tp vary depending on inferred redox states, but Ganne and Feng (2017) suggest that at ~ 2.7 – 2.8 Ga the lower value was ~ 1430° C. Thus, mantle plumes were not required to form all Archean boninitic suites but hydrous fluids probably were.

Barnes and Often (1990) originally inferred that magmas in the early Proterozoic Karasjok greenstone belt (Norway) erupted under shallow water conditions that favoured phreatomagmatic eruptions. Given the commonly volcaniclastic nature of the Karasjok suite world-wide, however, Barley et al (2000) later inferred that Karasjok type magmas were inherently volatile rich. Other Archean and post-Archean high-Mg volcaniclastic rock types, interpreted as either komatiites or picrites, have been accounted for as inherently hydrous magmas in recent years. For example, Triassic ultramafic arc picrites (liquid compositions with ~ 16. wt MgO but displaying up to 33 wt% Mg via accumulated olivine) comprising tuff breccia and lapilli and ash tuffs are interpreted by Milidragovic et al. (2016, 2018) as water-rich magmas that ascended rapidly through the mantle.

As discussed below, it is possible that phreatic processes did contribute to the production of fragmental GA lavas in the southern Murchison Domain, but it is clear that inherently volatile-rich magmas were being produced from mantle sources at about 2800 Ma. Ivanic et al.'s (2015) study of the dry c. 2813 Ma Windimurra Intrusive Complex and the hornblende-rich wet 2800 Ma Narndee Intrusive Complex demonstrated that the mantle beneath the Murchison was heterogeneously hydrated. Given the proximity of the two complexes, the relationship is most readily explained by a temporal heterogeneity where water was introduced into the upper mantle between the emplacement of the two complexes. Compositional similarities between some MM rocks and post-Archean Alaskan-type intrusions derived from hydrous arc magmas (e.g., Yuan et al., 2017) further suggests that wet mantle sources were common in the region.

4.3 Magma Mixing and Liquid Compositions

In addition to extensive large-scale Archean Intrusive Complexes such as the Windimurra and Narndee, smaller-scale intrusions are locally abundant in the Murchison, as in the Gabanintha area (Hallberg, 2000), and in the Mt Magnet and Mt Singleton areas (Lipple et al., 1983; Ivanic, 2018). Many of these smaller intrusions include olivine cumulate-rich horizons and the presence of ultramafic (MgO = 37 wt%) lava tubes at Mt. Singleton demonstrates that these cumulates were locally remobilized, as occurred with the "liquid/crystal mush" responsible for Troodos ultramafic pillows (Bailey et al., 1991). Similar ultramafic lavas of the Othris Ophiolite have MgO contents up to 33 wt% but, based on olivine compositions, are calculated to have had liquid compositions with only ~ 17 wt % MgO (Baziotis, 2017). As shown in Figure 10, the range of trace element compositions generated by olivine accumulation in the Othris Ophiolite closely matches that defined by the GA "Karasjok-type" rocks first reported by Barley et al. (2000). Such patterns are also found in other Archean and post-Archean picrites, as noted by Polat and Kerrich (2006).

The small intrusions observed in the Murchison would have provided excellent sites for the mixing of individual magma batches. Petrographic evidence demonstrates that ultramafic agglomerate in the Mt. Singleton suite contains numerous chromite-rich amoeboid fragments, likely representing cumulate material in a shallow magma chamber that was entrained when a new magma batch prompted eruption (Fig. 11a; sample MS 22B: 24.8 wt% MgO). Some other spinifex-textured spherical features appear to represent magma droplets entrained in related lavas, as in Figure 11b, although in some cases it is difficult to confirm whether spherical features reflect mixing or alteration (Fig. 11c). Figure 12 shows that there is a rapid decline in Cr contents with increasing Zr in the Youanmi Terrane volcanic data set (WACHEM, 2018) and in the Barberton low Al/Ti komatiite reference data sets (GEOROC, 2018). The trend is mainly matched by MM, MS and some GA data. The magma mixing inferred for the Mt Singleton agglomerate must have involved two low-Zr components. Similar mixing may have occurred in the GA suite but the distribution of many GA samples to the right side of the trend suggests mixing also occurred between low-Zr material containing excess Cr and high-Zr components.

Barley et al. (2000) reported that their sample GIR 135, with MgO contents of 22.5 wt%, was a weakly porphyritic flow top from the Gabanintha "Karasjok" suite, which is a key argument in support of the magmas being komatiitic. On the Cr or Ni vs Zr plot, however, the location of this sample to the right of the main Youanmi trend, suggests that it is actually a mixture of cumulate-bearing magma and a more evolved magma. The Gabanintha sample with most similar MgO content reported by Wyman and Kerrich (2012) has MgO = 23.6 wt% (sample ME15b). It contains abundant olivine phenocryst (± pyroxene) pseudomorphs, best observed in low magnification photomicrographic montages (Fig. 11d,e), and cannot represent a liquid magma composition.

Only 2 GA samples have Cr contents greater than the putative flow top. Using only the available data rather than an optimized theoretical end member, it is possible to create a simple mixing model based on Zr contents that replicates the mantle normalized plot of sample GIR 135 and produces relatively consistent values for compatible trace elements (Fig. 12). Rocks comparable to the evolved sample in the model are actually common in the Gabanintha area (WACHEM, 2018) in the Quinns Basalt Member. On the basis of this petrographic and chemical evidence, we suggest that the reported flow top sample cited by Barley et al. (2000) is actually a highly altered example of a cumulate olivine-bearing magma that underwent minor magma mixing and cannot be used to infer a primary magma liquid composition.

One plausible explanation for the distinct Cr vs Zr trend at Gabanintha is that the Quinns Basalt, or compositionally analogous magmas, represent the re-melting of hydrated tholeiitic crust at or near the sea floor. If early Singleton Formation volcanism occurred episodically in the Gabanintha area, then later magmas could locally melt the hydrated crust, forming "Icelanditic" melts that mixed with the newly arrived magmas. This scenario resolves the apparent contradiction presented by a comparison with the dry mantle source for the younger c. 2813 Ma Windimurra Intrusive Complex indicated by the study of Ivanic et al. (2015). The volcaniclastic nature of the GA suite noted by Barley et al. (2000) does not require that the parental magmas were inherently volatile-rich but corresponds instead with the assimilation of hydrated crust or magma mixing with small-volume melts derived from such crust.

4.4 Primary Magma Compositions versus Komatiite Classification

Relatively constant Al_2O_3/TiO_2 ratios over large ranges of TiO_2, Al_2O_3 and MgO contents indicate extensive olivine fractionation occurred (Fig. 6) in magmas of all three study areas. Based on petrographic observations and Harker diagrams such as MgO vs SiO_2, the liquid composition of the most mafic magmas in the GA and other sample suites lie in the region of ~ 16 wt% MgO. The available GA samples near this composition are highly altered but the distribution of relict oxides does not suggest a high phenocryst content. This inferred primary magma liquid composition is below the 18 wt% MgO criteria for komatiitic affinity favoured by Arndt et al. (2008), although they note that both higher and lower values have been used elsewhere. Given that Gabanintha ultramafic rocks are olivine cumulates and lack olivine spinifex textures, the Gabanintha suite, or similar rocks in the MM and MS suites do not actually meet any of the requirements of a komatiite classification favoured by most authorities in the field (e.g. Arndt et al., 2008 and references therein). In contrast, the scenario of subduction-related ~ 16 wt % MgO magmas producing ultramafic rock types (including tuffs) is increasingly recognized globally (Bailey et al., 1991; Milidragovic et al., 2016, 2018; Baziotis et al., 2017). It must also be noted that Szilas et al. (2012) assessed amphibolite metamorphic grade Mesoarchean rocks from SW Greenland that were compositionally similar to the Gabanintha suite and suggested that they originated by processes similar to those of post-Archean boninites.

4.5 Pyroxene Spinifex

When field evidence for a link between komatiite *ss*. and moderate-Mg mafic volcanics is lacking, textural characteristics such as acicular pyroxenes or pyroxene spinifex have commonly resulted in a default classification of those rocks as komatiitic basalt. This practice is not consistent with the requirement that basalts be linked spatially and genetically to true komatiites (Redman and Keays, 1985; Arndt, et al., 2008), but is understandable, given that basalts that do meet these criteria are often characterized by such textures (Cameron and Nisbet, 1982). Lowrey et al. (2017) have shown that in the Murchison Domain, and elsewhere, there are occurrences of platy pyroxene spinifex in basaltic to andesitic flows that mimic a texture previously considered to be diagnostic of olivine spinifex in true komatiites. This textural duplication has also likely led to field-based reports of komatiites in some parts of the Yilgarn and Pilbara Cratons where none are actually present (Lowrey et al., 2017).

The genesis and implications of pyroxene spinifex is presently the subject of considerable research, which has yet to resolve all of the factors that either permit or enhance pyroxene spinifex formation (Bouquain et al., 2009; 2014). Spectacular, metre-scale, occurrences of pyroxene spinifex have been reported from a range of magma compositions in the Nondweni greenstone belt (Wilson et al., 1989), including 'komatiities' (15-22 wt% MgO), 'komatiitic basalts' (7.5-15 wt% MgO) and 'komatiitic andesites' (8 -13 wt% MgO), which Riganti and Wilson (1995) likened to siliceous high-magnesium basalts (e.g., Sun, et al., 1989). Based on evidence for a shallow-water environment (stromatolites, evaporates) and the occurrence of similar pyroxene textures across a wide range of magma compositions, Wilson and Versfeld (1994) concluded that the spinifex formed as a result of environmental rather than compositional factors.

Wilson and Versfeld (1994) considered the Nondweni volcanic rocks to be petrogenetically similar to siliceous high-Mg volcanic types found in young volcanic settings and there are clear textural similarities between these occurrences. The fact that boninites had been overlooked in the Murchison Domain until reported by Wyman and Kerrich (2012) is probably due to their textural similarity with SHMB in the field. Comparisons between komatiitic basalts, SHMB and younger textural "analogues" have been presented for decades (e.g., Cameron and Nisbet, 1982*)*. Wood (1980) reported pyroxene spinifex texture in the unusual Cretaceous continental margin Kopi boninite (also illustrated in Wyman, 2018). A recent paper by Baziotis et al (2017), for example, displays skeletal and branching clinopyroxene dendrites or "microspinifex" (Arndt et al., 2008) in a high-Mg (11.5 – 13.7 wt% MgO), clinopyroxene-rich, dike of the Othris ophiolite. Comparable textures are reported from the Troodos ophiolite (Osozawa et al. 2012), similar to those reported in SHMBs in the Murchison domain (Lowrey et al., 2017). It is evident that the presence of pyroxene spinifex-textured rocks with MgO contents of ~ 8 to 16 wt% MgO in the Murchison domain do not provide unequivocal evidence of komatiitic basalts or the Komatiite lithofacies of Arndt et al. (2008).

4.6 Geodynamic Context

With the exception of mantle plume tectonics inferred from the presence of komatiites and (or) "komatiitic basalts" of varying pedigree, few (if any) Meso- or Neo-Archean greenstone belt geodynamic models have been developed on the basis of a single rock type in recent decades. The field observations and data from multiple rock types presented in this study provide important insights and constraints into the geodynamic evolution of the Yilgarn Craton at ~ 2800 Ma, although the apparent intra-cratonic setting of the Murchison boninites emphasizes that caution is required in comparisons with classic occurrences such as Cyprus or the Izu-Bonin-Marianna trench.

Models suggesting a coexistence or close association of Archean mantle plumes and subduction zones have become common since invoked for the Abitibi belt in Canada (Wyman et al., 1999 a,b) and mantle plume - subduction zone interactions are likely to have been quite numerous in the Phanerozoic, based on present day plume catalogues and plate reconstructions (Fletcher and Wyman, 2015). If the Gabanintha suite described by Barley et al. (2000) was in fact a variety of deep mantle plume-derived komatiite, then their model of plume ascent beneath a subduction-modified cratonic margin might possibly be adapted to account for the presence of so many rock types derived from hydrated mantle. Our results indicate, however, that the suite is not komatiitic and there is no *a priori* reason to invoke a mantle plume, particularly since the analogy drawn by Barley et al. (2000) with diamond-bearing rocks of Dachine, French Guiana, is likely based on a flawed assumption (Wyman et al., 2008; 2015). Prior to the assertion by Capdevila et al. (1999) that the Dachine rocks were komatiites, they had been classed as meta-kimberlite or meta-lamproite (Bailey, 1999 and references therein). Magee and Taylor (1999) suggested the rocks could actually be shoshonitic picrites. The latter model gains considerable credibility through comparisons with the Archean diamond-bearing shoshonitic lamprophyres and associated breccia's of the southern Superior Province, which Wyman et al. (2008; 2015) demonstrated had major and trace element compositions similar to the Dachine rocks.

Rather than being derived from depths of >250 km in the presence of residual majorite garnet as suggested by Barley et al. (2000), the HREE-depleted signature of some Singleton Formation magmas is more likely to have originated in a setting similar to that of "g-basalts" that have magma contributions from the upper mantle garnet stability field (Sacanni, 2015) and are associated with rifted continental margins (Dilek and Furnes, 2011). The Othris ophiolite of Greece may provide a relevant example. It has previously been described as including picrites, boninites and komatiite by Tsikouras et al. (2008) and hosts well developed pyroxene spinifex in some high-Mg rock types. The ultramafic rocks include suites with LREE enrichment, low Nb/La ratios and sporadic weak negative Ti, P, and Zr anomalies. Baziotis et al. (2017), however, argued based on olivine compositions that primary liquid compositions of the "komatiites" did not exceed 17 wt%, despite whole rock analyses extending to more than 30 wt% MgO. On this basis, they included the previously described komatiites with the Othris picrites. The boninites and associated rock types were emplaced in the narrow Pindos "oceanic strand" of the western Neothethys where Early Triassic rifting of continental crust was followed by Late Jurassic to early Tertiary subduction (Koutsovitis and Magganas, 2016; Dilek et al., 2008; Stampfli and Borel, 2002). Other possibly appropriate geodynamic analogues for the Murchison boninites, besides the Neotethys, may be other cases where such rocks are found in continental margins. The Kopi boninites of New Zealand and the SE Yukon examples described by Piercey et al (2001) have both been suggested to occur where spreading ridge propagation into a continental arc generated melting of refractory mantle that was previously metasomatised by subduction processes.

Wyman and Kerrich (2012) attempted to accommodate a ~ 2800 Ma "Norie mantle plume" into a geodynamic model for the Murchison Domain and the Yilgarn Craton based on prevailing models. At a minimum, however, the new results provide strong evidence against the long-lived plume models applied to the Murchison Domain and Yilgarn Craton. For example, Van Kranendonk et al. (2013) suggested that mantle plume impingement at 2820 – 2790 Ma set the stage for the generation of granitoids beginning at 2785 Ma via conductive heat transfer through thinned continental (cratonic) crust and attributed 2760 -2740 Ma magmatism to mixtures of crustal melts and the emplacement of mantle derived melts. This is a classic Yilgarn plume scenario but it is no longer tenable from the perspective of either mantle water contents or the compositions of rock types now recognized in the southern Murchison Domain.

The review of Alaskan-type intrusions by Himmelberg and Loney (1995) demonstrates that they have many features in common with intrusions of the Murchison Domain's Warreidar Intrusive Suite. They occur as numerous small intrusions with larger mafic-ultramafic complexes that may extend to about 10 km. This size range is far smaller than the largest mafic-ultramafic intrusions found in the Murchison Doman (30 – 80 km: Ivanic, 2016) but is similar the dimensions of the largest of Warreidar Suite intrusions (Ivanic, 2018). Combined with their geometry, the size range of post-Archean Alaskan-type intrusions suggest that many smaller bodies are subvolcanic feeder conduits, sills and shallow crustal magma chambers. The Alaskan-type rocks represent differentiated magmatic suites that encompass a wide compositional range, with MgO contents varying from ~ 43 wt% in dunitic zones to a few wt% in gabbros that, at least in part, evolved by flow differentiation in feeder conduits and sills (Himmelberg and Loney; 1995). This compositional range is matched by the Warreidar Suite, which extends from peridotite to gabbro and dolerite. In the original Alaskan type area, phlogopite and hornblende in ultramafic zones and the presence of hornblendite indicate they were hydrous magmas, while their trace element signatures imply a genetic association with Aleutian island arc lavas. The recurring combination of enriched LREE and negative Zr-Hf anomalies and comparatively low Th/La ratios evident in the Murchison intrusions and the Alaskan and North China Craton examples (Figure 10) do not appear to have been addressed directly in the literature. Yuan et al. (2017) do, however, favour a subduction-metasomatised lithospheric source rather than a modified asthenospheric wedge source for the Zhongtiao Mountain (North China Craton) examples, based on trace element and Nd-Hf isotopic data.

Given the arguments against crustal contamination, the HMA rocks of the MM suite are considered to be derived from asthenospheric mantle. Their similarities to “enriched” boninites and their association with other boninitic rocks and picrites correspond closely to the products derived from silica-enriched mantle sources of arc magmas (Bénard et al., 2017). There are several post-Archean localities where multiple boninitic types occur, such as the variably depleted Suite B and C of the Troodos ophiolite where both subduction initiation and an extended period of ridge subduction may have prolonged boninite magma formation (Osozawa et al., 2012).

Samples from the three study areas are plotted on two well-known plots applied to subduction-related rocks in Figure 13. The Ba/Th vs Th plot of Hawkseworth et al. (1997) in Figure 13a suggests that both fluids and sediment melts played a role in the enrichment of the magma sources of the Norie Group magmas and endorses a role for a sediments in the distinctive Yalgoginda (?) rocks that display very high Th contents. The lack of a correlation between Ba/Th and Th suggests that any effects of crustal contamination on magma compositions was minor. On a plot of Th/Yb vs Nb/Yb (Fig. 13b), the majority of Norie Group samples define a trend that parallels the mantle array, consistent with the observation of Smithies et al. (2018) for northern Murchison volcanic rocks. The high-Th HMA samples lie almost directly above the primitive mantle location, as might be expected from their normalized multi-element plots (Fig. 9e). Although some of the boninitic rocks display minor positive Zr-Hf anomalies, Norie Group samples do not fall within the region occupied by magmas that were strongly influenced by adakitic slab melts. In combination, these two plots suggest a subduction zone scenario similar to that found in most Phanerozoic arcs and show no evidence of systematic crustal contamination.

4.7 Yilgarn Model

The evidence presented here can be accounted for in a preliminary tectonic model for the ~ 2.8 Ga Yilgarn Craton involving subduction along its western margin. Several previous studies have argued for similar models. Myers (1995) was an early proponent who suggested that distinctive features and age distributions of the Narryer and Murchison (Youanmi) terranes required their assembly by a plate tectonic process that likely occurred at 2680 -2650 Ma, based on field relations such as tectonic interleaving and folding. Wilde et al. (1996) considered east-dipping upper crust reflectors, preserved 2790 Ma -2650 Ma greenstone sequences and post-tectonic granites as young as ~ 2580 Ma in the SW Yilgarn as evidence for Neoarchean terrane accretion. High HFSE 2750 Ma sanukitoid intrusions in the Murchison Domain and andesite-dacite-rhyolite volcanic rocks of the c. 2730 Marda complex in the Southern Cross Domain both suggest subduction-linked metasomatism above a subducting plate (Champion et al., 2002; Morris and Kirkland, 2014).

The rocks discussed here are mainly analogous to the almost continuous successions of the Norie and older Polelle Group of the northern Murchison Domain in what might be termed the “Norelle event”. Their association with a region of relatively isotopically juvenile crust (Fig. 1) suggests the possibility that extension within the older Yilgarn basement may have been tectonically linked to the formation of the magmas. Although interpreted domain and terrane boundaries in the Yilgarn have been modified frequently over the last few decades, this region of relatively juvenile crust has never been considered as a first-order terrane or domain boundary feature. Nonetheless, the geochemical and isotopic evidence suggests that complete attenuation of the existing cratonic crust may have occurred synchronously with the ca. 2815 Ma emplacement of the 38,000 km^3 Meeline suite of anhydrous tholeiitic magma intrusions (Ivanic, 2016).

The recognition of ~ 2790 Ma greenstone sequences in the SW Yilgarn implies that a subduction zone may have been present along the entire western margin of the craton. If so, then the Narryer Terrane, parts of the SW Yilgarn Terrane and (possibly) Murchison crust west of the isotopic juvenile zone probably did not arrive randomly, or independently accrete to the craton’s margin, but could represent a ribbon micro-continent. It is increasingly accepted that Yilgarn crust underwent extension prior to ~ 2720 Ma and that Youanmi-style crust extends to the eastern Yilgarn Craton (e.g., Van Krandendonk, 2013; Pawley et al., 2012). Based on detrital zircons in the Southern Cross Domain, Wyche et al. (2004) suggested that pre-3100 Ma Narryer crust may have been extended during deposition of pre-2700 Ma greenstone belts. Given that a ca. 2815 – 2800 Ma felsic volcanic rocks occur with undated spinifex-textured “komatiitic basalts” and dolerites and a ca. 2832 Ma monzogranite (Pawley et al., 2012 and references therein) in the NE Yilgarn, it is possible that subduction also occurred there at about the same time as the Norelle event, although further study is required.

Circum-cratonic subduction is commonly envisioned at the onset of local subduction or global plate tectonics in numerical models of Paleoarchean geodynamics. For example, if an early craton underwent gravitational collapse then subduction may be induced around its circumference (Rey et al., 2014). Rolf and Tackley (2011) found that convective stresses imposed by the asthenosphere on a craton embedded in thinner and weaker oceanic crust could also nucleate subduction initiation around the craton. Such local enforced subduction scenarios were probably not required by ~2800 Ma, given that the widespread evidence for subduction at 2750 Ma and onwards suggests a form of global plate tectonics was just about to emerge (e.g., Wyman, 2018 and references therein).

One possible scenario suggested by Phanerozoic “cratonic” boninites involves the propagation of an ocean spreading centre toward the Yilgarn Craton. As shown in Figure 13a, such a scenario could account for Norelle-like rocks in the eastern Yilgarn and the rapid ~ 2800 Ma transition from wet to dry mantle sources for intrusions coeval with Norie Group volcanism. The spreading centre would first induce extension in the craton but if the ridge propagated past the Yilgarn then plate convergence and subduction could result. The modal can account for the possible occurrence of subduction on both sides of the Yilgarn craton if the propagating rift “calved off” the thin margins of the craton but only produced crustal extension in the core.

Interestingly, there is evidence to suggest that such double subduction zones occurred elsewhere at around the time of magmatism in the Norie and Lower Polelle Groups. The interpretation of Percival et al. (2012) for the onset of Superior Province consolidation bears striking similarities to the contemporaneous Yilgarn (prior to the development of the Eastern Goldfields Terrane) as illustrated in Figure 13b. The analogy and potential correlation are made even more compelling by the fact that volcanism at 2830 Ma – 2800 Ma was much less common globally than it was after 2750 Ma (Wyman, 2018). In Figure 13b a hypothetical ~ 2830 Ma Yilgarn has been added to the NW margin of the Superior Province. In this scenario, the Narryer Terrane corresponds to the Hudson Bay Terrane, the “Norelle” magmatism equates to 2830 Ma – 2800 Ma Hayes River magmatism in the Oxford-Stull Domain (OSD; see also Metsaranta and Houle, 2017a, b), the upper Polelle Group corresponds to the ~ 2722 Ma Knee Lake volcanics and sedimentary rocks of the OSD and the Youanmi Terrane matches the ~ 3000 Ma North Caribou Terrane (Percival et al., 2012; Corkery et al., 2000). Moreover, the OSD contains significant intrusive complexes extending at least from 2808 Ma to the 2735 Ma “Ring of

Fire” mafic-ultramafic intrusion, which is a feeder to ultramafic to felsic sills and volcanic rocks (Mungall et al., 2010; Metsaranta and Houle, 2017a,b).

A similar “inward-dipping” double slab subduction event (Holt et al., 2017) may have recurred again in the Yilgarn after 2750 Ma. Van Kranendonk et al. (2013) described andesites from the upper Polelle and showed that they chemically resembled some Phanerozoic arc-related andesites. They cautioned that such signatures might be generated by mantle plume-related crustal melting. The latter scenario now appears less viable for those particular rocks given the re-assessment here of the putative 2830 Ma mantle plume. Van Kranendonk et al. (2013) also reported pyroxene-spinifex bearing ~ 2725 Ma volcanic rocks in the Murchison Domain’s Glen Group where 4 of 5 samples have MgO between 5.7 and 8.3 wt% MgO and the other has 17.5 wt% MgO. Primary amphiboles occur in associated gabbros but were interpreted as the product of contamination by hydrous crust. All of these rocks need to be re-evaluated in the light of findings in Lowrey et al. (2017) and the present work. Many, but not all, Yilgarn researchers infer subduction events starting after 2750 Ma in the eastern Yilgarn prior to or broadly coeval with the onset of classic mantle plume-derived komatiitic magmatism in the Kalgoorlie Terrane (Standing, 2008; Czarnota et al., 2010; Begg et al., 2010). This corresponds to a global upswing in volcanism, crustal growth and cratonization (Wyman, 2018 and references therein). On this basis, it is possible that the Yilgarn Craton underwent two periods of “inward-dipping” double slab subduction between 2830 Ma and final cratonization around 2650 Ma.

5. Conclusions

The results of this study provide major new insights into mid- to late-Archean magmatism in the Murchison Domain and have important geodynamic implications for the Yilgarn Craton. The new evidence strongly suggests that the so-called Karasjok komatiite suite of the Gabanintha area is actually derived from parental magmas with primary liquid compositions having ~ 16 wt% MgO. The subduction-like signatures were not acquired at shallow crustal levels and instead represent features established in their mantle sources near the shallowing lithosphere-asthenosphere boundary; they are more appropriately termed arc picrites. The Gabanintha suite is just one of several hydrous magma types found in the Murchison Domain but it predates the transition from comparatively dry to wet mantle documented by the study of intrusive complexes by Ivanic et al. (2015). The suite likely acquired water from hydrated crust, which was locally remelted to generate Fe-Ti rich tholeiitic basaltic andesites. In contrast, the later large-scale wet Narndee Intrusive Complex and smaller intrusions with Alaska-type affinities suggest widespread hydration of mantle sources, probably including the asthenosphere and lithosphere.

In cratons where magmatism intrudes existing crust there can be uncertainties about the origin of "arc-like" andesites and felsic volcanic rocks. The high-Mg andesites reported here display mantle-like Zr/Y combined with LREE enrichment and strong normalized depletions of both Nb-Ta and Zr-Hf, which are not observed in andesites plausibly derived from plume- generated remelting of cratonic crust. In combination with previously published data, our results suggest a period of subduction likely occurred at ~ 2830 Ma – 2790 Ma along the Yilgarn western margin and possibly slightly earlier along the eastern margin. The absence of a "Norie plume" during this interval indicates that younger Polelle and Glen Group volcanism were not products of mantle plume incubation as often hypothesized for evolved magmas of the Yilgarn Craton. Instead, they likely represented subduction-related volcanism that was broadly coeval with subduction events in the eastern Yilgarn. The occurrence of apparent intra-cratonic boninites in the Murchison Domain may be most appropriately compared to Phanerozoic occurrences linked to continental rifting, ribbon continents and associated short-lived narrow oceans. The 40 m.y. duration of the magmatism represented by the Norie and Lower Polelle Groups is similar to that shown by the southern Abitibi belt in Canada and demonstrates that the concept of short-lived subduction events controlled by slab break off, as envisioned by Moyen and van Hunen (2012), was probably more applicable to older greenstone belts.

Based on the paucity of ~ 2815 Ma volcanism world-wide, the events documented in the Norie Group need not signify a global set of interacting plates as found on the modern Earth but may slightly predate such a configuration at ~ 2750 Ma (Wyman, 2018). A propagating ridge model for Norie and Lower Polelle Group magmatism in the Murchison Domain is suggested by similarities with Neotheyan boninites occurrences. A more speculative possible correlation of the Mesoarchean Yilgarn with the North Caribou Terrane of the Superior Province would not necessarily negate the propagating ridge scenario. The correlation is far from proven at this point but provides some support for arguments that the Yilgarn was part of a Superia supercontinent in the Paleoproterozoic (Söderlund et al., 2010).

Acknowledgments

This study was supported with funding from Australian Research Council grant LP130100722 and the Geological Survey of Western Australia. Ramelius Resources Ltd. and Volker Gartz are thanked for access and assistance with drill core samples from Mt. Magnet. Discussions with Jack Lowrey and early access to the Ninghan map sheet provided by Tim Ivanic helped to greatly improve the paper.

References

Ameen, S.M.M., Wilde, S.A., 2018. Multiple sources for Archean granitoids in the Yalgoo area, Yilgarn Craton, Western Australia: Geochemical and isotopic evidence. Precambrian Research 314, 76-110.

Arndt, N., Lesher, C.M., Barnes, S.J., 2008. Komatiite. Cambridge University Press, New York.

Bailey, D.G., Langdon, G.S., Malpas, J., Robinson, P.T., 1991. Ultramafic and related lavas from the Margi area, Troodos ophiolite; in Cyprus Crustal Study Project: initial Report, Holes CY-1 and 1 A. Geological Survey of Canada, Paper 90-20, 187-202.

Bailey, L.M., 1999. An unusual diamond-bearing talc schist from the Dachine area of French Guiana. Unpublished MSc thesis. Queen's University, Canada, p. 161.

Barley, M.E., Kerrich, R., Reudavy, I., Xie, Q., 2000. Late Archaean Ti-rich, Al-depleted komatiites and komatiitic volcaniclastic rocks from the Murchison Terrane in Western Australia. Australian Journal of Earth Sciences 47, 873-883.

Barnes, S.-J., Often, M., 1990. Ti-rich komatiites from northern Norway. Contributions to Mineralogy and Petrology 105, 42-54.

Barnes, S.J., Van Kranendonk, M.J., 2014. Archean andesites in the east Yilgarn craton, Australia: Products of plume-crust interaction? Lithosphere 6, 80-92.

Begg, G.C., Griffin, W.L., O'Reilly, S.Y., Napatov, L.M., 2010. Archean cratonic architecture: implications for the Yilgarn and Superior Provinces., Yilgarn-Superior Workshop – Abstracts, Fifth Archean Symposium, 10 September 2010, pp. 1–3. Geological Survey of Western Australia Record 2010/20.

Bénard, A., Arculus, R.J., Nebel, O., Ionov, D.A., McAlpine, S.R.B., 2017. Silica-enriched mantle sources of subalkaline picrite-boninite-andesite island arc magmas. Geochimica et Cosmochimica Acta 199, 287-303.

Baziotis, I., Economou-Eliopoulos, M., Asimow, P.D., 2017. Ultramafic lavas and high-Mg basaltic dykes from the Othris ophiolite complex, Greece. Lithos 288, 231-247.

Bouquain, S., Arndt, N.T., Hellebrand, E., Faure, F., 2009. Crystallochemistry and origin of pyroxenes in komatiites. Contributions to Mineralogy and Petrology 158, 599-617.

Bouquain, S., Arndt, N.T., Faure, F., Libourel, G., 2014. An experimental study of pyroxene crystallization during rapid cooling in a thermal gradient: application to komatiites. Solid Earth 5, 641-650.

Cameron, W.E., Nisbet, E.G., 1982. Phanerozoic analogues of komatiitic basalts, in: Crawford, A.J. (Ed.), Boninites and Related Rocks. Unwin Hyman, London, pp. 29-50.

Capdevila, R., Arndt, N., Letendre, J., Sauvage, J.-F., 1999. Diamonds in volcaniclastic komatiite from French Guiana. Nature 399, 456-458.

Cassidy, K., Champion, D.C., Krapež, B., Barley, M.E., Brown, S.J.A., Blewett, R.S., Groenewald, P.B., Tyler, I.M., 2006. A revised geological framework for the Yilgarn Craton, Western Australia: Western Australia Geological Survey, Record 2006/8, 14p..

Champion, D.C., Cassidy, K.F., Budd, A., 2002. Granites of the northern Murchison province: their distribution, age, geochemistry, petrogenesis, relationship with mineralisation, and implications for tectonic environment., in: Cassidy, K.F., Champion, D.C., McNaughton, N.J., Fletcher, I.R., Whitaker, A.J., Bastrakova, I.V., Budd, A.R. (Eds.), Characterisation and Metallogenic Significance of Archaean Granitoids of the Yilgarn Craton, Western Australia. Minerals and Energy Research Institute of Western Australia (MERIWA), Report No. 222, 514p.

Champion, D.C., Cassidy, K.F., 2007. An Overview of the Yilgarn Craton and its Crustal Evolution in: Bierlein, F.P., C.M, K.-R. (Eds.), Kalgoorlie'07 Geoscience Australia Record 2007/14. Commonwealth of Australia, Kalgoorlie, pp. 8-13.

Champion, D.C., Huston, D.L., 2016. Radiogenic isotopes, ore deposits and metallogenic terranes: Novel approaches based on regional isotopic maps and the mineral systems concept. Ore Geology Reviews 76, 229-256.

Cooper, L.B., Plank, T., Arculus, R.J., Hauri, E.H., Hall, P.S., Parman, S.W., 2010. High-Ca boninites from the active Tonga Arc. J. Geophys. Res. 115, B10206.

Corkery, M.T., Cameron, H.D.M., Lin, S., Skulski, T., Whalen, J.B., Stern, R.A., 2000. Geological Investigations in the Knee Lake Belt (Parts of NTS 53L), Report of Activities 2000, Manitoba Geological Survey, pp. 129-136.

Czarnota, K., Champion, D.C., Goscombe, B., Blewett, R.S., Cassidy, K.F., Henson, P.A., Groenewald, P.B., 2010. Geodynamics of the eastern Yilgarn Craton. Precambrian Research 183, 175-202.

Dilek, Y., Furnes, H., 2011. Ophiolite genesis and global tectonics: Geochemical and tectonic fingerprinting of ancient oceanic lithosphere. Geological Society of America Bulletin 123, 387-411.

Dilek, Y., Furnes, H., Shallo, M., 2008. Geochemistry of the Jurassic Mirdita Ophiolite (Albania) and the MORB to SSZ evolution of a marginal basin oceanic crust. Lithos 100, 174-209.

Elliott, T., Plank, T., Zindler, A., White, W., Bourdon, B., 1997. Element transport from slab to volcanic front at the Mariana arc. Journal of Geophysical Research: Solid Earth 102, 14991-15019.

Falloon, T.J., Danyushevsky, L.V., 2000. Melting of Refractory Mantle at 1·5, 2 and 2·5 GPa under Anhydrous and H2O-undersaturated Conditions: Implications for the Petrogenesis of High-Ca Boninites and the Influence of Subduction Components on Mantle Melting. Journal of Petrology 41, 257-283.

Falloon, T.J., Danyushevsky, L.V., Crawford, T.J., Maas, R., Woodhead, J.D., Eggins, S.M., Bloomer, S.H., Wright, D.J., Zlobin, S.K., Stacey, A.R., 2007. Multiple mantle plume components involved in the petrogenesis of subduction-related lavas from the northern termination of the Tonga Arc and northern Lau Basin: Evidence from the geochemistry of arc and backarc submarine volcanics. Geochemistry, Geophysics, Geosystems 8, Q09003.

Fitton, J.G., Saunders, A.D., Norry, M.J., Hardarson, B.S., Taylor, R.N., 1997. Thermal and chemical structure of the Iceland plume. Earth and Planetary Science Letters 153, 197-208.

Fletcher, M., Wyman, D.A., 2015. Mantle plume–subduction zone interactions over the past 60 Ma. Lithos 233, 162-173.

Ganne, J., Feng, X., 2017. Primary magmas and mantle temperatures through time. Geochemistry, Geophysics, Geosystems 18, 872-888.

GEOROC, 2018. Geochemistry of Rocks of the Oceans and Continents. Max Plank Institute for Chemistry. http://georoc.mpch-mainz.gwdg.de/georoc/

Gibson, H.L., Allen, R.L., Riverin, G., Lane, T.E., 2007. The VMS Model: Advances and Application to Exploration Targeting, in: Milkereit, B. (Ed.), Proceedings of Exploration 07: Fifth Decennial International Conference on Mineral Exploration, pp. 713-730.

GSWA, 2014. Murchison, 2014: Geological Information Series. Geological Survey of Western Australia. Unique Identifier DCA1FB4D-6234-4360-AFA4-0B9B59F4658A.

Hallberg, J.A., 2000. Notes to accompany the Hallberg Murchison 1:25 000 Geology Dataset, 1989–1994; J. A. Hallberg and Associates: Western Australia Geological Survey, Record 2000/20, parts 1–6. Western Australia Geological Survey.

Hanski, E., Huhma, H., Rastas, P., Kamenetsky, V.S., 2001. The Palaeoproterozoic Komatiite–Picrite Association of Finnish Lapland. Journal of Petrology 42, 855-876.

Hawkesworth, C.J., Turner, S.P., McDermott, F., Peate, D.W., van Calsteren, P., 1997. U-Th Isotopes in Arc Magmas: Implications for Element Transfer from the Subducted Crust. Science 276, 551.

Hermann, J., Rubatto, D., 2009. Accessory phase control on the trace element signature of sediment melts in subduction zones. Chemical Geology 265, 512-526.

Himmelberg, G.R., Loney, R.A., 1995. Characteristics and petrogenesis of Alaskan-type ultramafic-mafic intrusions, southeastern Alaska. US Geological Survey Professional Paper 1564.

Hirai, Y., Yoshida, T., Okamura, S., Tamura, Y., Sakamoto, I., Shinjo, R., 2018. Breakdown of residual zircon in the Izu arc subducting slab during backarc rifting. Geology 46, 371-374.

Holt, A.F., Royden, L.H., Becker, T.W., 2017. The dynamics of double slab subduction. Geophysical Journal International 209, 250-265.

Ivanic, T., 2016. A field guide to the mafic–ultramafic intrusions of the Youanmi Terrane, Yilgarn Craton: Geological Survey of Western Australia, Record 2016/6, 61p.

Ivanic, T.J., 2018, Ninghan, WA Sheet 2339: Geological Survey of Western Australia, 1:100 000 Geological Series

Ivanic, T.J., Nebel, O., Jourdan, F., Faure, K., Kirkland, C.L., Belousova, E.A., 2015. Heterogeneously hydrated mantle beneath the late Archean Yilgarn Craton. Lithos 238, 76-85.

Ivanic, T.J., Wingate, M.T., Van Kranendonk, M.J., Kirkland, C.L., Wyche, S., 2010. Age and significance of voluminous mafic-ultramafic magmatic events in the Murchison Domain, Yilgarn Craton, in: Tyler, I.M., Knox-Robinson, C.M. (Eds.), 5th International Archean Symposium Perth, Australia, pp. 75-77.

Ivanic, T.J., Van Kranendonk, M.J., Kirkland, C.L., Wyche, S., Wingate, M.T.D., Belousova, E.A., 2012. Zircon Lu–Hf isotopes and granite geochemistry of the Murchison Domain of the Yilgarn Craton: Evidence for reworking of Eoarchean crust during Meso-Neoarchean plume-driven magmatism. Lithos 148, 112-127.

Jónasson, K., 2005. Magmatic evolution of the Heioarsporour ridge, NE-Iceland. Journal of Volcanology and Geothermal Research 147, 109-124.

Koutsovitis, P., Magganas, A., 2016. Boninitic and tholeiitic basaltic lavas and dikes from dispersed Jurassic East Othris ophiolitic units, Greece: petrogenesis and geodynamic implications. International Geology Review 58, 1983-2006.

Kuritani, T., Yokoyama, T., Kitagawa, H., Kobayashi, K., Nakamura, E., 2011. Geochemical evolution of historical lavas from Askja Volcano, Iceland: Implications for mechanisms and timescales of magmatic differentiation. Geochimica et Cosmochimica Acta 75, 570-587.

Langmuir, C.H., Bézos, A., Escrig, S., Parman, S.W., 2006. Chemical Systematics and Hydrous Melting of the Mantle in Back-Arc Basins, Back-Arc Spreading Systems: Geological, Biological, Chemical, and Physical Interactions. AGU Geophysical Monograph 166, pp. 87-146.

Lesher, C.M., Arndt, N.T., 1995. REE and Nd isotope geochemistry, petrogenesis and volcanic evolution of contaminated komatiites at Kambalda, Western Australia. Lithos 34, 127-157.

Lipple, S.L., Baxter, J.L., Marston, R.J., 1983. Ninghan Western Australia, 1:250,000 Geological Series Explanatory Notes, Geological Survey of Western Australia, Perth, Australia, p. 23.

Lowrey, J.R., Wyman, D.A., Ivanic, T.J., Smithies, R.H., Mass, R., 2019. Archean boninite-like rocks of the Western Yilgarn: geochemistry and genesis (in preparation).

Lowrey, J.R., Ivanic, T.J., Wyman, D.A., Roberts, M.P., 2017. Platy Pyroxene: New Insights into Spinifex Texture. Journal of Petrology 58, 1671-1700.

Magee, C.W., Taylor, W.R., 1999. Diamond and Chromite Geochemical Constraints on the Nature of the Dachine Complex, French Guiana, Annual Report 1998/8, Petrochemistry and Experimental Petrology. Research School of Earth Sciences, Australian National University, 85.

Martin, D.M., Hocking, R.M., Riganti, R.M.A., Tyler, I.M., 2015. Geological map of Western Australia, 1:2 500 000 (14th edition). Geological Survey of Western Australia.

McDonough, W.F., Sun, S.S., 1995. The composition of the Earth. Chemical Geology 120, 223-253.

Metsaranta, R., Houle, M.G., 2017. Precambrian geology of the Highbank Lake area, “Ring of Fire” region, Ontario— central sheet. Ontario Geological Survey Preliminary Map P. 3805; Geological Survey of Canada, Open File 8201. Scale 1:100,000.

Metsaranta, R.T., M., H., 2017. Precambrian geology of the Highbank Lake area, “Ring of Fire” region, Ontario— southern sheet. Ontario Geological Survey Preliminary Map P. 3806; Geological Survey of Canada, Open File 8202. Scale 1:100,000.

Milidragovic, D., Chapman, J.B., Bichlmaier, S., Canil, D., Zagorevski, A., 2016. H2O-driven generation of picritic melts in the Middle to Late Triassic Stuhini arc of the Stikine terrane, British Columbia, Canada. Earth and Planetary Science Letters 454, 65-77.

Milidragovic, D., Zagorevski, A., Weis, D., Joyce, N., Chapman, J.B., 2018. Picrite “Intelligence” from the Middle-Late Triassic Stikine arc: Composition of mantle wedge asthenosphere. Lithos 308-309, 446-461.

Mole, D.R., Barnes, S.J., Yao, Z., White, A.J.R., Maas, R., Kirkland, C.L., 2018. The Archean Fortescue large igneous province: A result of komatiite contamination by a distinct Eo-Paleoarchean crust. Precambrian Research 310, 365-390.

Mole, D.R., Fiorentini, M.L., Thebaud, N., Cassidy, K.F., McCuaig, T.C., Kirkland, C.L., Romano, S.S., Doublier, M.P., Belousova, E.A., Barnes, S.J., Miller, J., 2014. Archean komatiite volcanism controlled by the evolution of early continents. Proceedings of the National Academy of Sciences 111, 10083-10088.

Morris, P.A., Kirkland, C.L., 2014. Melting of a subduction-modified mantle source: A case study from the Archean Marda Volcanic Complex, central Yilgarn Craton, Western Australia. Lithos 190–191, 403-419.

Moyen, J.-F., van Hunen, J., 2012. Short-term episodicity of Archaean plate tectonics. Geology 40, 451-454.

Mungall, J.E., Harvey, J.D., Balch, S.J., Hamilton, M.A., 2010. Eagle's Nest: A Magmatic Ni-Sulfide Deposit in the James Bay Lowlands, Ontario, Canada, in: R.J. Goldfarb, E.E. Marsh, Monecke, T. (Eds.), The Challenge of Finding New Mineral Resources: Global Metallogeny, Innovative Exploration and New Discoveries Volume II: Zinc-Lead, Nickel-Copper-PGE, and Uranium. Society of Economic Geologists, pp. 539–557.

Myers, J.S., 1995. The generation and assembly of an Archaean supercontinent: evidence from the Yilgarn craton, Western Australia. Geological Society, London, Special Publications 95, 143-154.

Nebel, O., Arculus, R.J., Ivanic, T.J., Nebel-Jacobsen, Y.J., 2013. Lu–Hf isotopic memory of plume–lithosphere interaction in the source of layered mafic intrusions, Windimurra Igneous Complex, Yilgarn Craton, Australia. Earth and Planetary Science Letters 380, 151-161.

Osozawa, S., Shinjo, R., Lo, C.-H., Jahn, B.-m., Hoang, N., Sasaki, M., Ishikawa, K.i., Kano, H., Hoshi, H., Xenophontos, C., Wakabayashi, J., 2012. Geochemistry and geochronology of the Troodos ophiolite: An SSZ ophiolite generated by subduction initiation and an extended episode of ridge subduction? Lithosphere 4, 497-510.

Pawley, M.J., Wingate, M.T.D., Kirkland, C.L., Wyche, S., Hall, C.E., Romano, S.S., Doublier, M.P., 2012. Adding pieces to the puzzle: episodic crustal growth and a new terrane in the northeast Yilgarn Craton, Western Australia. Australian Journal of Earth Sciences 59, 603-623.

Pearce, J.A., 2008. Geochemical fingerprinting of oceanic basalts with applications to ophiolite classification and the search for Archean oceanic crust. Lithos 100, 14-48.

Pearce, J.A., Robinson, P.T., 2010. The Troodos ophiolitic complex probably formed in a subduction initiation, slab edge setting. Gondwana Research 18, 60-81.

Percival, J.A., Skulski, T., Sanborn-Barrie, M., Stott, G.M., Leclair, A.D., Corkery, M.T., Boily, M., 2012. Geology and Tectonic Evolution of the Superior Province, Canada in: Percival, J.A., Cook, F.A., Clowes, R.M. (Eds.), Tectonic Styles in Canada: The LITHOPROBE Perspective. Geological Association of Canada Special Paper 49, pp. 321-378.

Piercey, S.J., Murphy, D.C., Mortensen, J.K., Paradis, S., 2001. Boninitic magmatism in a continental margin setting, Yukon- Tanana terrane, southeastern Yukon, Canada. Geology 29, 731-734.

Polat, A., Kerrich, R., 2006. Reading the Geochemical Fingerprints of Archean Hot Subduction Volcanic Rocks: Evidence for Accretion and Crustal Recycling in a Mobile Tectonic Regime. Archean Geodynamics and Environments. American Geophysical Union Monograph 164, 189-213.

Portnyagin, M.V., Danyushevsky, L.V., Kamenetsky, V.S., 1997. Coexistence of two distinct mantle sources during formation of ophiolites: a case study of primitive pillow-lavas from the lowest part of the volcanic section of the Troodos Ophiolite, Cyprus. Contributions to Mineralogy and Petrology 128, 287-301.

Reagan, M.K., Ishizuka, O., Stern, R.J., Kelley, K.A., Ohara, Y., Blichert-Toft, J., Bloomer, S.H., Cash, J., Fryer, P., Hanan, B.B., Hickey-Vargas, R., Ishii, T., Kimura, J.-I., Peate, D.W., Rowe, M.C., Woods, M., 2010. Fore-arc basalts and subduction initiation in the Izu-Bonin-Mariana system. Geochem. Geophys. Geosyst. 11, Q03X12.

Redman, B.A., Keays, R.R., 1985. Archaean basic volcanism in the Eastern Goldfields Province, Yilgarn Block, Western Australia. Precambrian Research 30, 113-152.

Rey, P.F., Coltice, N., Flament, N., 2014. Spreading continents kick-started plate tectonics. Nature 513, 405-408.

Riganti, A., Wilson, A.H., 1995. Geochemistry of the mafic/ultramafic volcanic associations of the Nondweni greenstone belt, South Africa, and constraints on their petrogenesis. Lithos 34, 235-252.

Rolf, T., Tackley, P.J., 2011. Focussing of stress by continents in 3D spherical mantle convection with self-consistent plate tectonics. Geophysical Research Letters 38, L18301.

Saccani, E., 2015. A new method of discriminating different types of post-Archean ophiolitic basalts and their tectonic significance using Th-Nb and Ce-Dy-Yb systematics. Geoscience Frontiers 6, 481-501.

Said, N., Kerrich, R., 2009. Geochemistry of coexisting depleted and enriched Paringa Basalts, in the 2.7 Ga Kalgoorlie Terrane, Yilgarn Craton, Western Australia: Evidence for a heterogeneous mantle plume event. Precambrian Research 174, 287-309.

Schaefer, S.J., Morton, P., 1991. Two komatiitic pyroclastic units, Superior Province, northwestern Ontario: their geology, petrography, and correlation. Canadian Journal of Earth Sciences 28, 1455-1470.

Sigmarsson, O., Steinthórsson, S., 2007. Origin of Icelandic basalts: A review of their petrology and geochemistry. Journal of Geodynamics 43, 87-100.

Smithies, R.H., Champion, D.C., 2000. The Archaean high-Mg diorite suite: Links to Tonalite-Trondhjemite-Granodiorite magmatism and implications for early Archaean crustal growth. Journal of Petrology 41, 1653-1671.

Smithies, R.H., Ivanic, T.J., Lowrey, J.R., Morris, P.A., Barnes, S.J., Wyche, S., Lu, Y.-J., 2018. Two distinct origins for Archean greenstone belts. Earth and Planetary Science Letters 487, 106-116.

Söderlund, U., Hofmann, A., Klausen, M.B., Olsson, J.R., Ernst, R.E., Persson, P.-O., 2010. Towards a complete magmatic barcode for the Zimbabwe craton: Baddeleyite U–Pb dating of regional dolerite dyke swarms and sill complexes. Precambrian Research 183, 388-398.

Stampfli, G.M., Borel, G.D., 2002. A plate tectonic model for the Paleozoic and Mesozoic constrained by dynamic plate boundaries and restored synthetic oceanic isochrons. Earth and Planetary Science Letters 196, 17-33.

Standing, J.G., 2008. Terrane amalgamation in the Eastern Goldfields Superterrane, Yilgarn Craton: Evidence from tectonostratigraphic studies of the Laverton Greenstone Belt. Precambrian Research 161, 114-134.

Stone, W.E., Crocket, J.H., Dickin, A.P., Fleet, M.E., 1995. Origin of Archean ferropicrites: geochemical constraints from the Boston Creek Flow, Abitibi greenstone belt, Ontario, Canada. Chemical Geology 121, 51-71.

Stone, W.E., Deloule, E., Stone, M.S., 2003. Hydromagmatic amphibole in komatiitic, tholeiitic and ferropicritic units, Abitibi greenstone belt, Ontario and Québec: evidence for Archaean wet basic and ultrabasic melts. Mineralogy and Petrology 77, 39-65.

Sun, S.-S., Nesbitt, R.W., McCulloch, M.T., 1989. Geochemistry and petrogenesis of siliceous high magnesian basalts of the Archaean and early Proterozoic, in: Crawford, A.J. (Ed.), Boninites and Related Rocks. Unwin Hyman, pp. 148-173.

Szilas, K., Næraa, T., Scherstén, A., Stendal, H., Frei, R., van Hinsberg, V.J., Kokfelt, T.F., Rosing, M.T., 2012. Origin of Mesoarchaean arc-related rocks with boninite/komatiite affinities from southern West Greenland. Lithos 144–145, 24-39.

Tatsumi, Y., Kogiso, T., 2003. The subduction factory: its role in the evolution of the Earth’s crust and mantle. Geological Society, London, Special Publications 219, 55-80.

Taylor, R.N., 1990. Geochemical stratigraphy of the Troodos extrusive sequence: temporal developments of a spreading centre magma chamber, Troodos 87: Ophiolites and Oceanic Lithosphere. Cyprus Geological Survey Department, Nicosia, pp. 187-202.

Taylor, R.N., Nesbitt, R.W., Vidal, P., Harmon, R.S., Auvray, B., Croudace, I.W., 1994. Mineralogy, Chemistry, and Genesis of the Boninite Series Volcanics, Chichijima, Bonin Islands, Japan. Journal of Petrology 35, 577-617.

Thompson, M.J., Watchorn, R.B., Bonwick, C.M., Frewin, M.O., Goodgame, V.R., Pyle, M.J., MacGeehan, P.J., 1990. Gold deposits of Hill 50 Gold Mine NL at Mount Magnet, in: Hughes, F.E. (Ed.), Geology of the Mineral Deposits of Australia and Papua New Guinea The Australasian Institute of Mining and Metallurgy, Melbourne, pp 221-241.

Tsikouras, B., Pe-Piper, G., Piper, D.J.W., Hatzipanagiotou, K., 2008. Triassic rift-related komatiite, picrite and basalt, Pelagonian continental margin, Greece. Lithos 104, 199-215.

Van Kranendonk, M.J., Ivanic, T.J., 2009. A new lithostratigraphic scheme for the northeastern Murchison Domain, Yilgarn Craton. Geological Survey of Western Australia Annual Review 07-08, 35-53.

Van Kranendonk, M.J., Ivanic, T.J., Wingate, M.T.D., Kirkland, C.L., Wyche, S., 2013. Long-lived, autochthonous development of the Archean Murchison Domain, and implications for Yilgarn Craton tectonics. Precambrian Research 229, 49-92.

WACHEM, 2018. Geological Survey of Western Australia, Western Australian Geochemistry database (WACHEM) http://www.dmp.wa.gov.au/GeoChem-Extract-Geochemistry-1559.aspx

Wang, Z., Wilde, S.A., Wan, J., 2010. Tectonic setting and significance of 2.3–2.1Ga magmatic events in the Trans-North China Orogen: New constraints from the Yanmenguan mafic–ultramafic intrusion in the Hengshan–Wutai–Fuping area. Precambrian Research 178, 27-42.

Watkins, K.P., Hickman, A.H., 1990. Geological evolution and mineralization of the Murchison Province, Western Australia, p. 267p.

Wilde, S.A., Middleton, M.F., Evans, B.J., 1996. Terrane accretion in the southwestern Yilgarn Craton: evidence from a deep seismic crustal profile. Precambrian Research 78, 179-196.

Wilson, A.H., Versfeld, J.A., Hunter, D.R., 1989. Emplacement, crystallization and alteration of spinifex-textured komatiitic basalt flows in the Archaean Nondweni greenstone belt, southern Kaapvaal Craton, South Africa. Contributions to Mineralogy and Petrology 101, 301-317.

Wilson, A.H., 2003. A new class of silica enriched, highly depleted komatiites in the southern Kaapvaal Craton, South Africa. Precambrian Research 127, 125-141.

Wilson, A.H., Adrian Versfeld, J., 1994. The early Archaean Nondweni greenstone belt, southern Kaapvaal Craton, South Africa, Part II. Characteristics of the volcanic rocks and constraints on magma genesis. Precambrian Research 67, 277-320.

Wingate, M.T.D., Kirkland, C.L., Ivanic, T.J., 2013. 198228: volcaniclastic metasandstone, Mount Singleton, Geochronology Record 1105; Geological Survey of Western Australia, 4p.

Witt, W.K., Cassidy, K.F., Lu, Y.-J., Hagemann, S.G., 2018. The tectonic setting and evolution of the 2.7 Ga Kalgoorlie–Kurnalpi Rift, a world-class Archean gold province. Mineralium Deposita.

Woelki, D., Regelous, M., Haase, K.M., Romer, R.H.W., Beier, C., 2018. Petrogenesis of boninitic lavas from the Troodos Ophiolite, and comparison with Izu–Bonin–Mariana fore-arc crust. Earth and Planetary Science Letters 498, 203-214.

Wood, C.P., 1980. Boninite at a continental margin. Nature 288, 692-694.

Wyche, S., Nelson, D.R., Riganti, A., 2004. 4350–3130 Ma detrital zircons in the Southern Cross Granite–Greenstone Terrane, Western Australia: implications for the early evolution of the Yilgarn Craton. Australian Journal of Earth Sciences 51, 31-45.

Wyman, D., 2018. Do cratons preserve evidence of stagnant lid tectonics? Geoscience Frontiers 9, 3-17.

Wyman, D.A., Bleeker, W., Kerrich, R., 1999. A 2.7 Ga plume, proto-arc, to arc transition and the geodynamic setting of the Kidd Creek deposit: evidence from precise ICP MS trace element data, in: Hannington, M.D., Barrie, C.T. (Eds.), Economic Geology Monograph 10 The Giant Kidd Creek Volcanogenic Massive Sulfide Deposit, Western Abitibi Subprovince, Canada, pp. 511-528.

Wyman, D.A., Kerrich, R., Polat, A., 2002. Assembly of Archean cratonic mantle lithosphere and crust: Plume-arc interaction in the Abitibi-Wawa subduction-accretion complex. Precambrian Research 115, 37-62.

Wyman, D.A., Kerrich, R., Groves, D.I., 1999. Lode gold deposits and Archean mantle plume-island arc interaction, Abitibi subprovince, Canada. Journal of Geology 107, 715-725.

Wyman, D., Kerrich, R., 2009. Plume and arc magmatism in the Abitibi subprovince: Implications for the origin of Archean continental lithospheric mantle. Precambrian Research 168, 4-22.

Wyman, D.A., Kerrich, R., 2012. Geochemical and isotopic characteristics of Youanmi terrane volcanism: The role of mantle plumes and subduction tectonics in the western Yilgarn Craton. Australian Journal of Earth Sciences 59, 671-694.

Wyman, D.A., O'Neill, C., Ayer, J.A., 2008. Evidence for Modern-Style Subduction to 3.1 Ga: A Plateau – Adakite – Gold (Diamond) Association, in: Condie, K.C., Pease, V. (Eds.), When Did Plate Tectonics Begin on Planet Earth? GSA Special Paper 440. Geological Society of America, pp. 129-148.

Wyman, D.A., Hollings, P., 2006. Late Archean convergent margin volcanism in the Superior Province: A comparison of the Blake River Group and Confederation Assemblage, in: Benn, K., Mareschal, J.-C., Condie, K. (Eds.), American Geophysical Union Monograph 164, Archean Geodynamics and Environments, pp. 215 – 238.

Wyman, D.A., Hollings, P., Conceição, R.V., 2015. Geochemistry and radiogenic isotope characteristics of xenoliths in Archean diamondiferous lamprophyres: Implications for the Superior Province cratonic keel. Lithos 233, 111-130.

Yuan, L., Zhang, X., Yang, Z., Lu, Y., Chen, H., 2017. Paleoproterozoic Alaskan-type ultramafic–mafic intrusions in the Zhongtiao mountain region, North China Craton: Petrogenesis and tectonic implications. Precambrian Research 296, 39-61.

Zibra, I 2015, Mount Magnet, WA Sheet 2441: Geological Survey of Western Australia, 1:100 000 Geological Series.

Zibra, I., Gessner, K., Smithies, H.R., Peternell, M., 2014. On shearing, magmatism and regional deformation in Neoarchean granite-greenstone systems: Insights from the Yilgarn Craton. Journal of Structural Geology 67, 253-267.

FIGURE CAPTIONS

Fig. 1. A) Tectonic scheme of Yilgarn Craton adapted from Witt et al. (2018) and Martin et al. (2015). B) Terrane map of the Yilgarn Craton contoured for 2-stage depleted-mantle model age (T_{DM}^2) based on the Nd-isotopic compositions of 442 felsic igneous rocks (Smithies et al, 2018).

Fig. 2. A summary of zircon U-Pb geochronology results from the western Yilgarn Craton dated from 3000 until 2700 Ma. Data from GSWA (2014) and screened for maximum analytical uncertainty less than 25 Ma.

Fig. 3. Stratigraphic cross sections for the Mount Singleton area and the Saturn Pit area at Mt Magnet, based on Ivanic (2018) and Zibra (2015).

Fig. 4. A) Hyaloclastite and B) Variolitic mafic flow in outcrop, Mount Singleton locality. C) Magma tubes at Mount Singleton: right side shows full tube structure; left beneath hammer: half drained and collapsed tube. D) Coarse string beef spinifex textured high-Mg basalts from the vicinity of Hy Brasil homestead, eastern part of Mount Magnet greenstone belt, E) Relict acicular texture, now defined by actinolite, in chloritized and carbonate-altered “Alaskan-type” intrusions (Hill 50 area, Mount Magnet); F) bedded volcaniclastic rocks near the Hy Brazil homestead.

Fig. 5. Harker variation diagrams Mt Singleton and Mt Magnet samples versus Gabanintha area rocks and samples from the WACHEM database for Youanmi Terrane igneous rocks.

Fig. 6. Al-Ti-Mg systematics of Mt Singleton and Mount Magnet samples compared to the Gabanintha suite.

Fig. 7. Incompatible element systematics of Mt Singleton and Mount Magnet samples compared to the Gabanintha suite and other Youanmi igneous rocks.

Fig. 8. Middle to Heavy REE fractionation versus Light to Middle REE fractionation and REE-Zr relationships of Mt Singleton and Mount Magnet samples compared to the Gabanintha suite.

Fig. 9. Primitive Mantle-normalized multi-element plots for Mt Magnet and Mt Singleton. Normalizing factors from McDonough and Sun (1995). Narndee Intrusive sample in panel A is the whole rock from which Ivanic et al. (2015) obtained Hf = 0 in zircon. Panel D: WR17= Warriedar area

intrusion; WS85 from 2.2 Ga North China Craton Intrusion, Wang et al., 2010; 87GH35A Olivine clinopyroxenite, Alaska, Himmleberg and Loney, 1995; Panel J: Margi = sample from Margi locality, Troodos Ophiolite.

Fig. 10. A and B) Primitive-mantle normalized multi-element plots for rocks of the Gabanintha area. C) Comparison of mafic-ultramafic Gabanintha rocks and Triassic Othris ophiolite. See text for discussion. Data in A from WACHEM (2018), in B from Barley et al. (2000), and Wyman and Kerrich (2012). Othris data from Baziotis et al. (2017). Normalizing factors from McDonough and Sun (1995).

Fig. 11. Arc Picrites of the Murchison Domain. A. Ultramafic agglomerate, Mt Singleton (Sample MS 22B) showing chromite-rich amoeboid fragments and smaller fragments. Image is a montage in both transmitted *and* reflected plane polarized light. Blue tinge on opaques on the right is an artefact of the montage production. B mixing of two related magma batches, both now exhibiting pyroxene spinifex. C Spherical to patchy regions distinguished surrounding from rock by matrix colour. Both regions display pyroxene spinifex texture and some crystals cross the boundaries between the regions. B and C both in unpolarized light. D and E (also shown as inset in D). Gabanintha sample ME15B in transmitted light showing pseudomorphs of accumulated olivine ± pyroxene in a fine-grained, opaque-rich, matrix. See text for discussion.

Fig. 12. **Top.** Cr vs Zr plot for MM, MS and GA samples compared to Youanmi data base from WACHEM and Barberton Komatiites from the Georoc data base (http://georoc.mpch-mainz.gwdg.de/georoc/). High – Cr to high-Zr mixing trend for GA samples may result from local re-melting of tholeiitic crust. See text. Highlighted GA samples: Grey circle GIR-204; Red circle GIR-135; Black circle 81928. Blue circle ME 15B (c.f. Fig 11). Highlighted MS sample: Green square MS 22B (c.f. Fig. 11). Data from Barley et al. (2000), Wyman and Kerrich (2012) and WACHEM. **Middle.** Mantle-normalized (McDonough and Sun, 1995) multi-element plots for sample GIR-135 and Zr-based mixing comparison between samples GIR-204 and 81298. Data from Barley et al. (2000) and WACHEM. **Bottom.** Comparison of select compatible trace elements for the Zr-based model and Barley et al. (2000) GIR-135 "flow top" sample. See text for discussion.

Fig. 13. A) Ba/Th vs Th plot after Hawkesworth et al. (1997). Most samples appear to have been derived from sources influenced by either hydrous fluids of sediment melts, but not both. B) Th/Yb vs Nb/Yb plot (Pearce, 2008; Smithies et al. 2018) showing that the Norie Group samples mainly define an array that is sub-parallel to the Mantle Array, except for those samples in A) for which

sediment melts are implicated. Yilgarn TTG field and Archean Crust from Smithies et al. (2018). Red letters are igneous rocks for which slab melts have previously been invoked in their sources. S= Setouchi High-Mg andesites (Tatsumi et al., 2003); M = Marda Complex Youanmi Terrane (Morris and Kirkland, 2014); A= Abitibi adakites (Wyman et al., 2002); P = Pilbara high-Mg diorites (Smithies and Champion, 2000), B= pre-“granite bloom” Abitibi Blake River assemblage including tholeiites, which define a trend similar to the main Norie trend, and transitional calc alkaline rocks. The latter are attributed to a mix of tholeiite sources and slab melts where the red “B” is located near the start of the slab melt trend (Wyman published and unpublished data). Based on these two plots, there is no indication of a substantial slab melt or crustal contamination influence on the Norie Group magmas.

Fig. 14. **A)** Propagating Spreading Centre model where a spreading centre tip (red colours) propagates from upper right to lower left causing short-lived subduction on the east and west margins of ~ 2.8 Ga Yilgarn. Inferred eastern Yilgarn 2840 Ma past subduction age linked to 2832 Ma monzogranite, etc (see text). At ~ 2800 Ma, western Yilgarn setting changes from extension to subduction as the spreading centre moves away from craton. Approximate ages inferred from dry to wet mantle transition. See text. **B)** Hypothetical addition of the 2830 Ma Yilgarn Craton to a double subduction setting at the NW margin of the Superior Province accretion model of Percival et al. (2012). HBT: Hudson Bay Terrane; OSD: Oxford-Stull Domain; NCT: North Caribou Terrane; RAT: Rivière Arnaud Terrane; WRT: Winnipeg River Terrane; MT= Marmion Terrane; OT: Opatica Terrane; WAT: Wawa-Abitibi Terrane; MRVT: Minnesota River Valley Terrane; HT: Hawk Terrane.; GI: Guano Island Sequence (< 2728 Ma Strike-slip Basin Deposit, slightly extended from Percival et al., 2006). Bottom panel: present-day scales of the Yilgarn Craton and NCT with Nd isotopic anomaly region and OSD stippled.

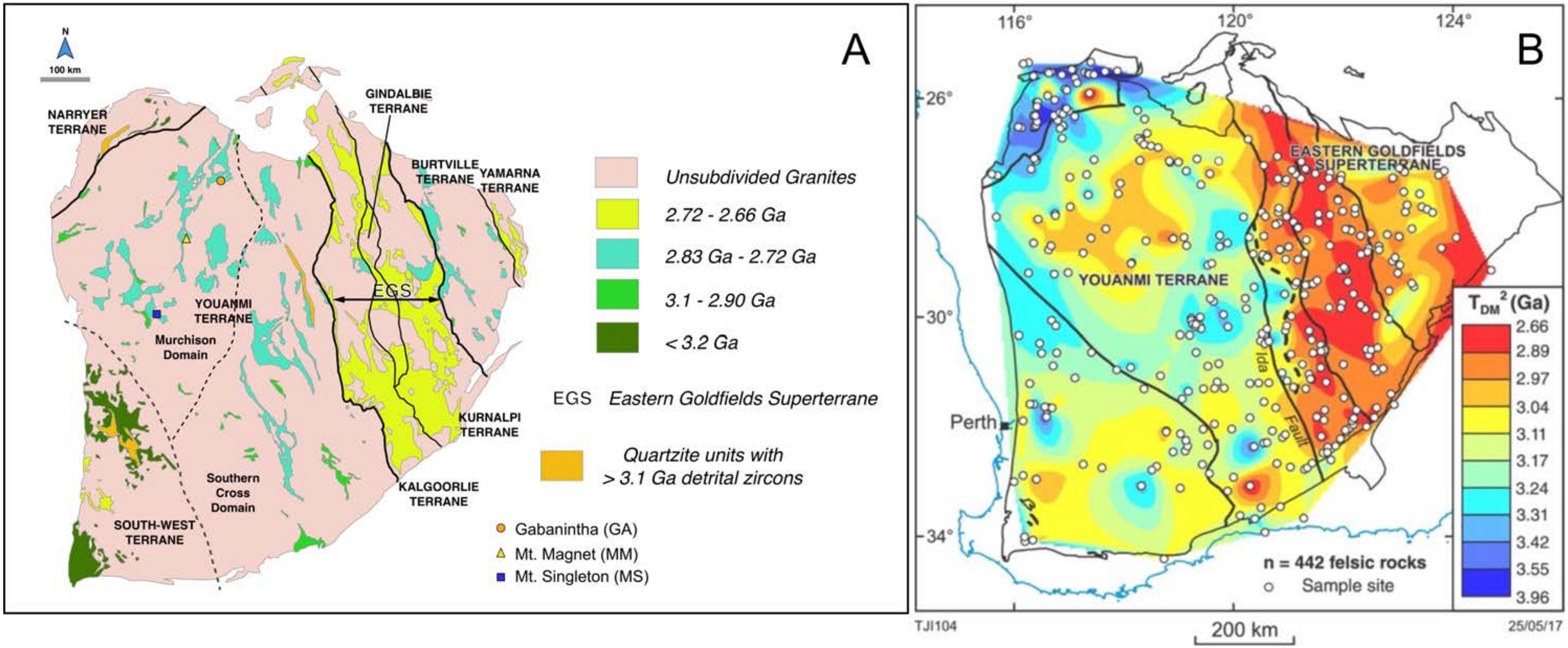
A
N
100 km
NARRYER TERRANE
GINDALBIE TERRANE
BURTVILLE TERRANE
YAMARNA TERRANE
YOUANMI TERRANE
Murchison Domain
EGS
KURNALPI TERRANE
Southern Cross Domain
KALGOORLIE TERRANE
SOUTH-WEST TERRANE
Unsubdivided Granites
2.72 - 2.66 Ga
2.83 Ga - 2.72 Ga
3.1 - 2.90 Ga
< 3.2 Ga
EGS Eastern Goldfields Superterrane
Quartzite units with > 3.1 Ga detrital zircons
Gabanintha (GA)
Mt. Magnet (MM)
Mt. Singleton (MS)
B
116°
120°
124°
26°
30°
34°
EASTERN GOLDFIELDS SUPERTERRANE
YOUANMI TERRANE
Ida Fault
Perth
T_{DM}^2 (Ga)
2.66
2.89
2.97
3.04
3.11
3.17
3.24
3.31
3.42
3.55
3.96
n = 442 felsic rocks
Sample site
TJI104
200 km
25/05/17

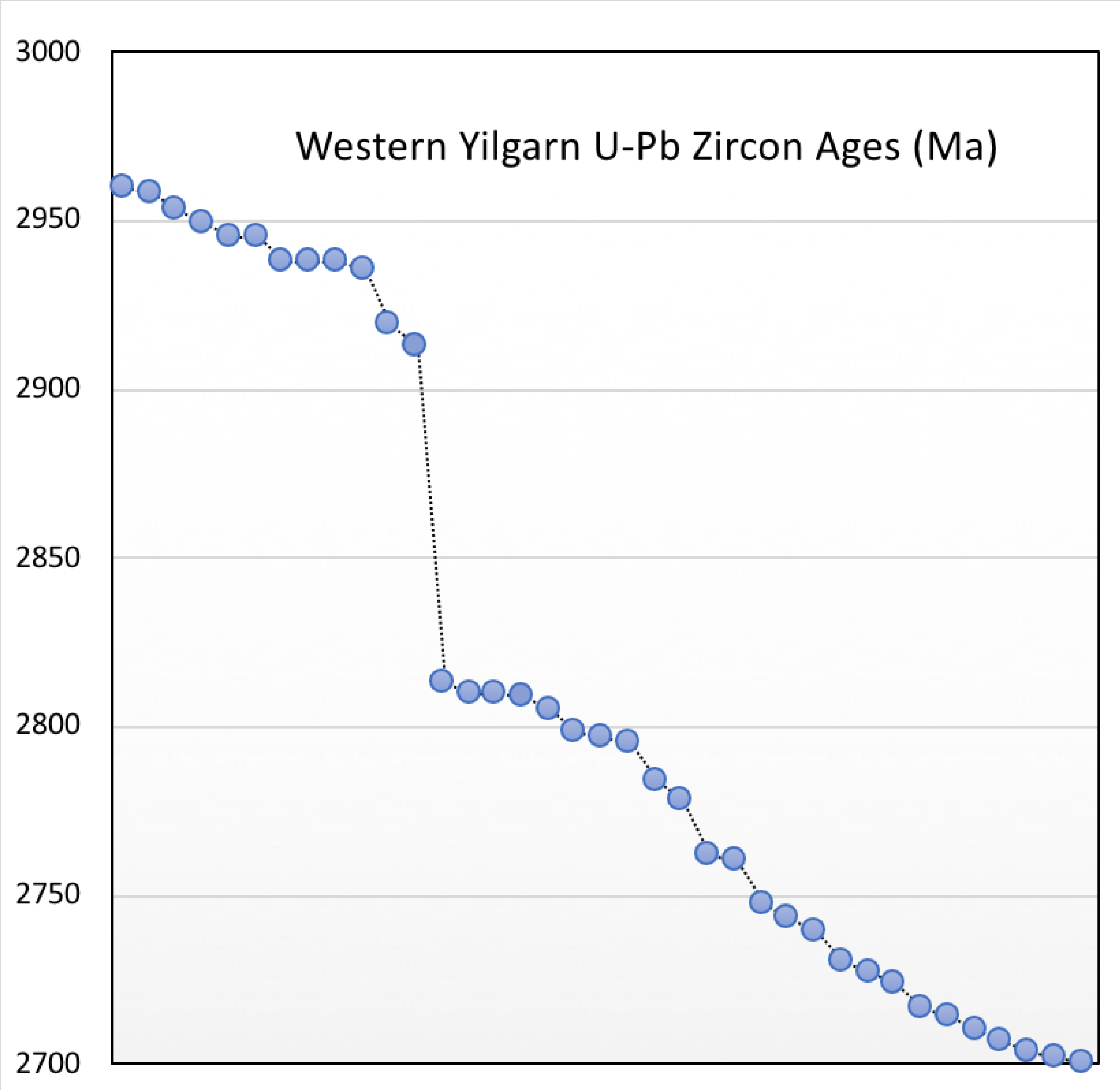
Western Yilgarn U-Pb Zircon Ages (Ma)
3000
2950
2900
2850
2800
2750
2700

Mt. Magnet Cross Section

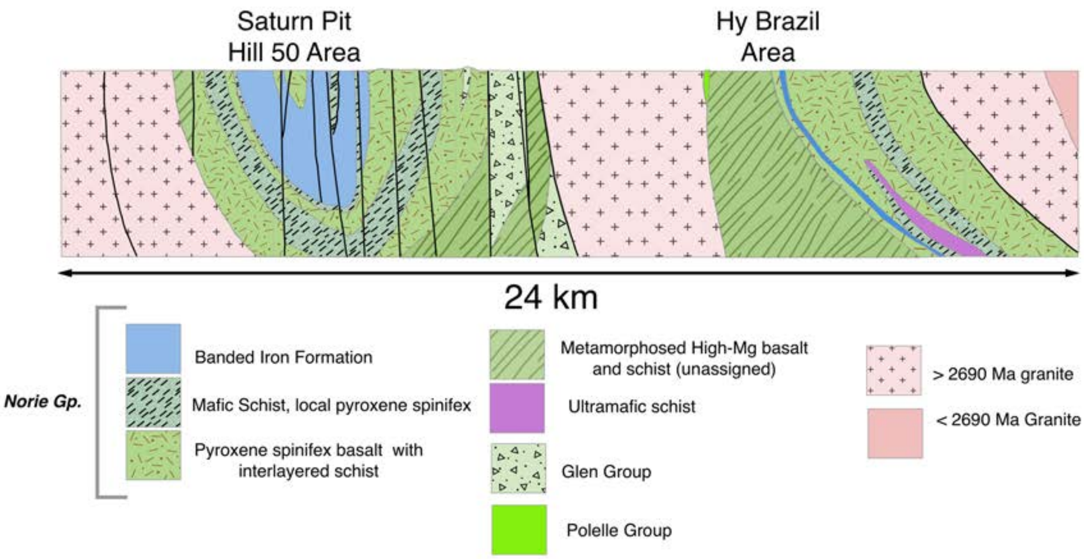

Mt. Singleton Cross Section

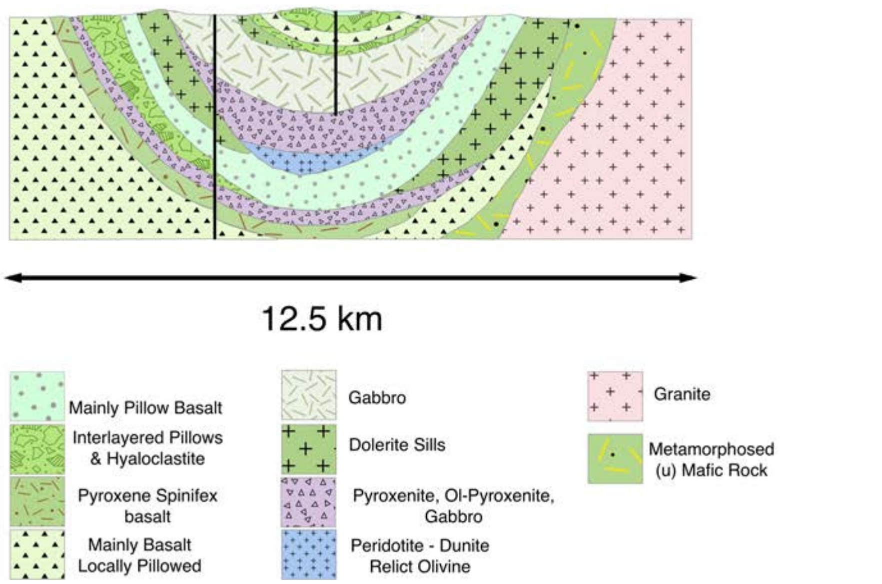

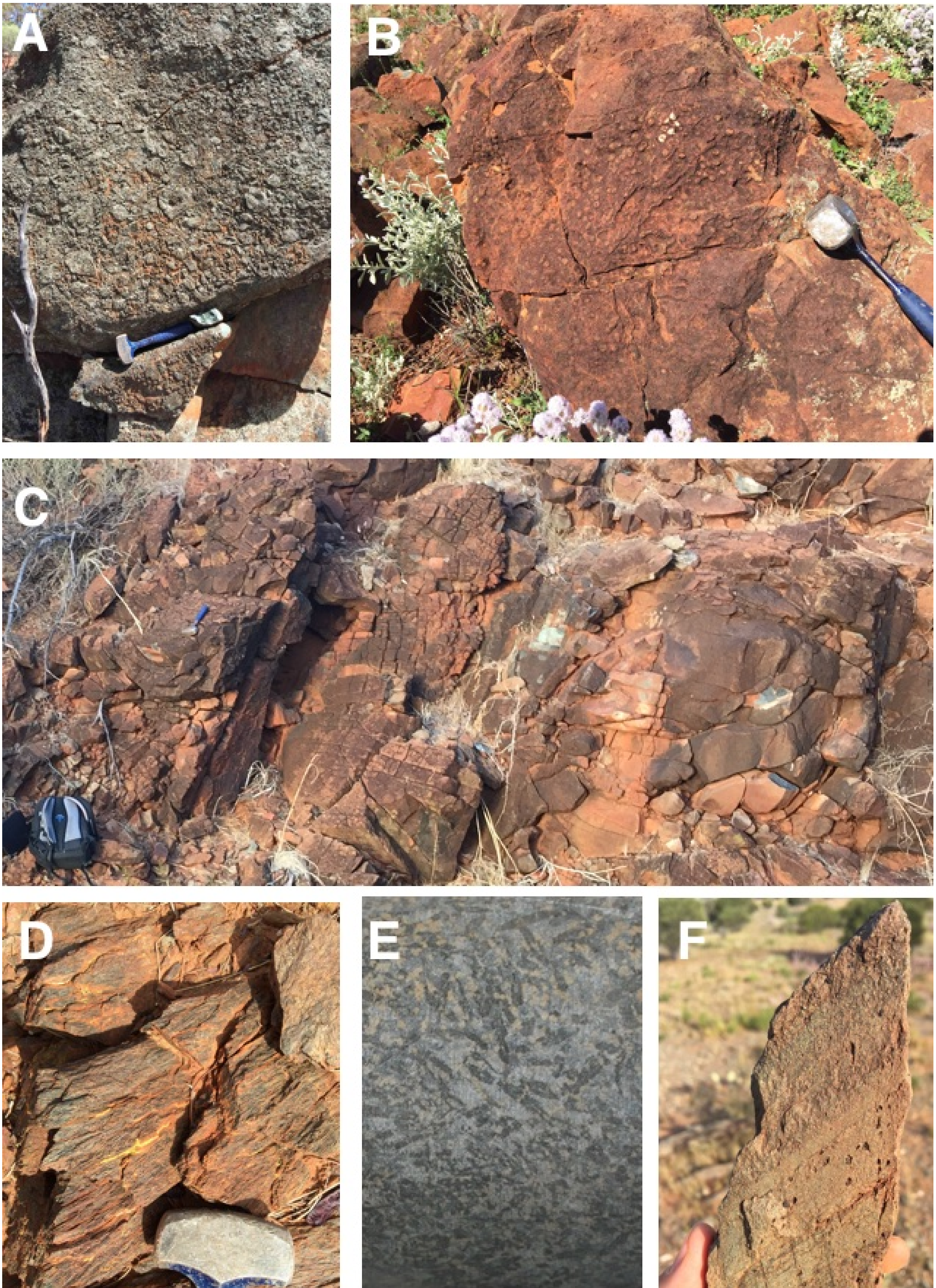
A
B
C
D
E
F

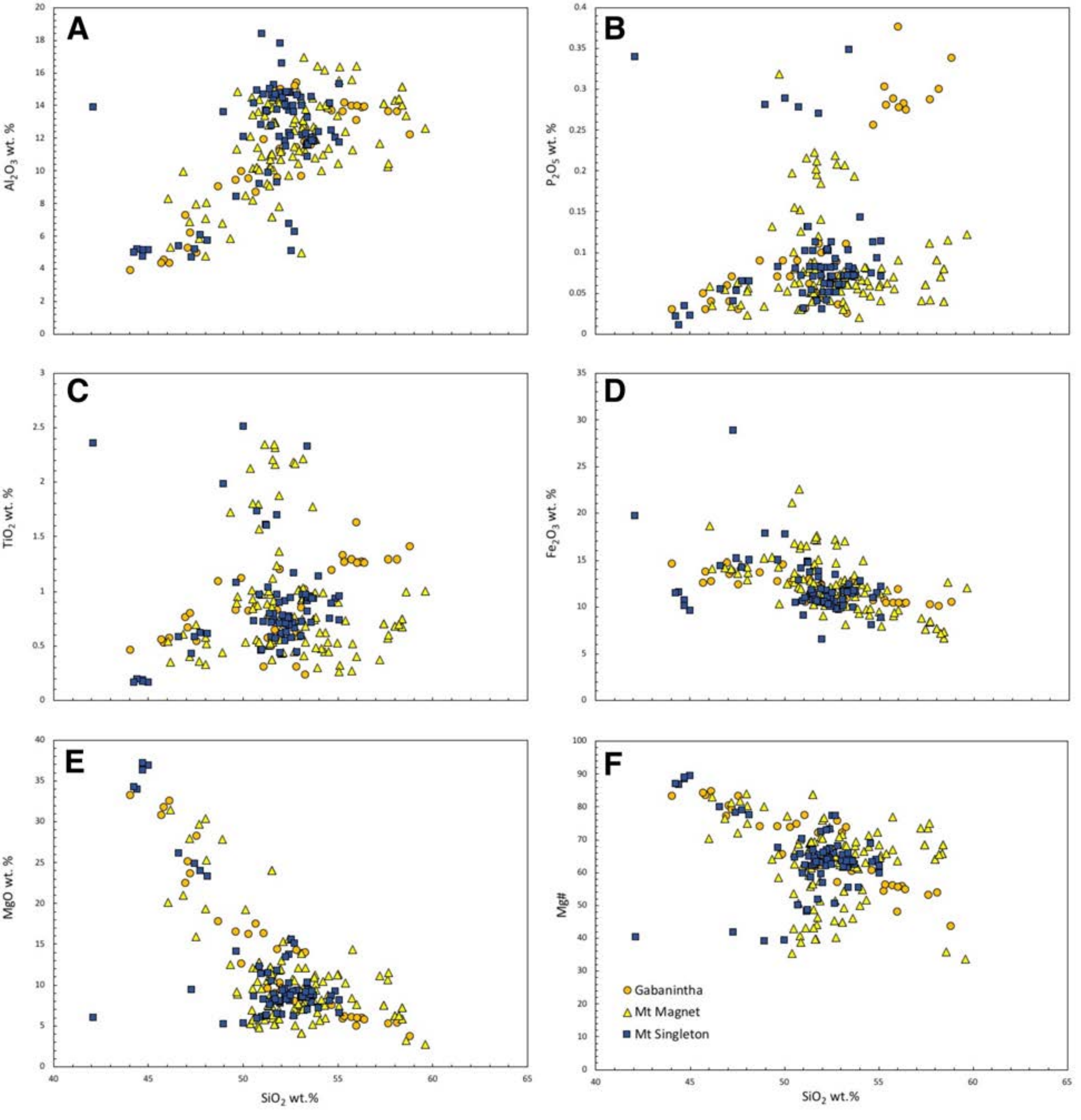
A
B
C
D
E
F
Al2O3 wt. %
P2O5 wt. %
TiO2 wt. %
Fe2O3 wt. %
MgO wt. %
Mg#
SiO2 wt.%
SiO2 wt.%
Gabanintha
Mt Magnet
Mt Singleton

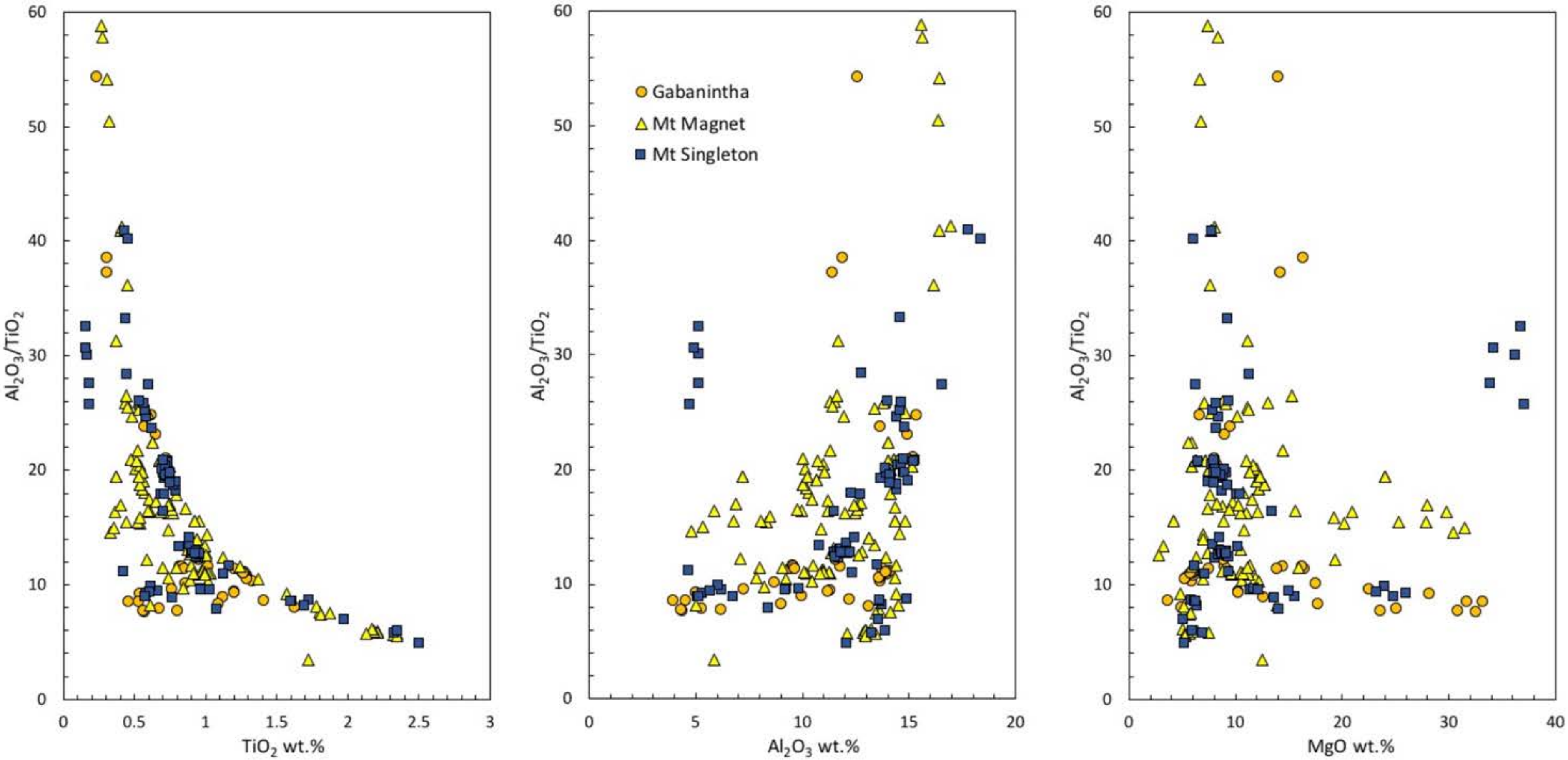

Gabanintha
Mt Magnet
Mt Singleton
Al_2O_3/TiO_2
TiO_2 wt.%
Al_2O_3 wt.%
MgO wt.%

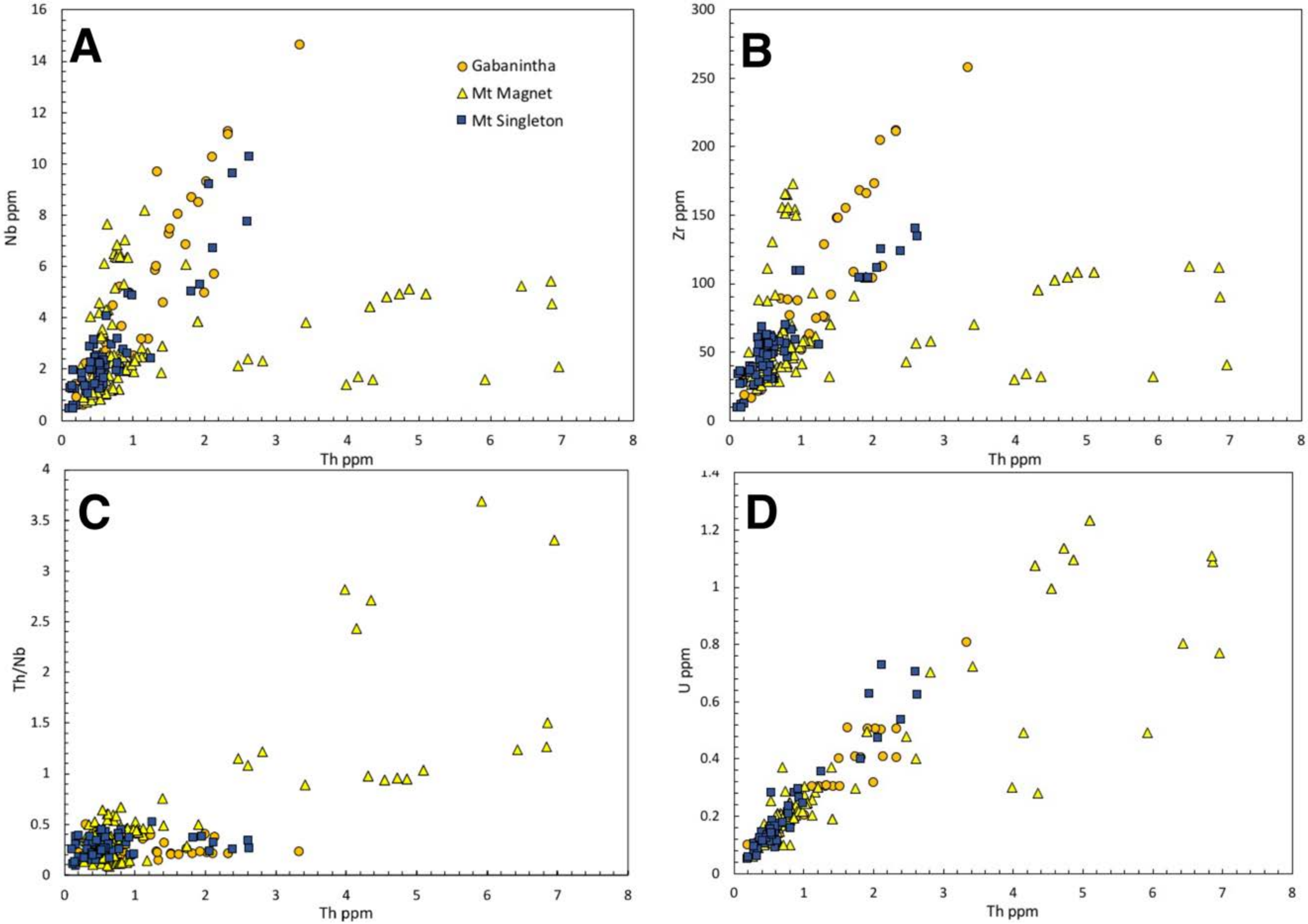

A
Gabanintha
Mt Magnet
Mt Singleton
Nb ppm
Th ppm
B
Zr ppm
Th ppm
C
Th/Nb
Th ppm
D
U ppm
Th ppm

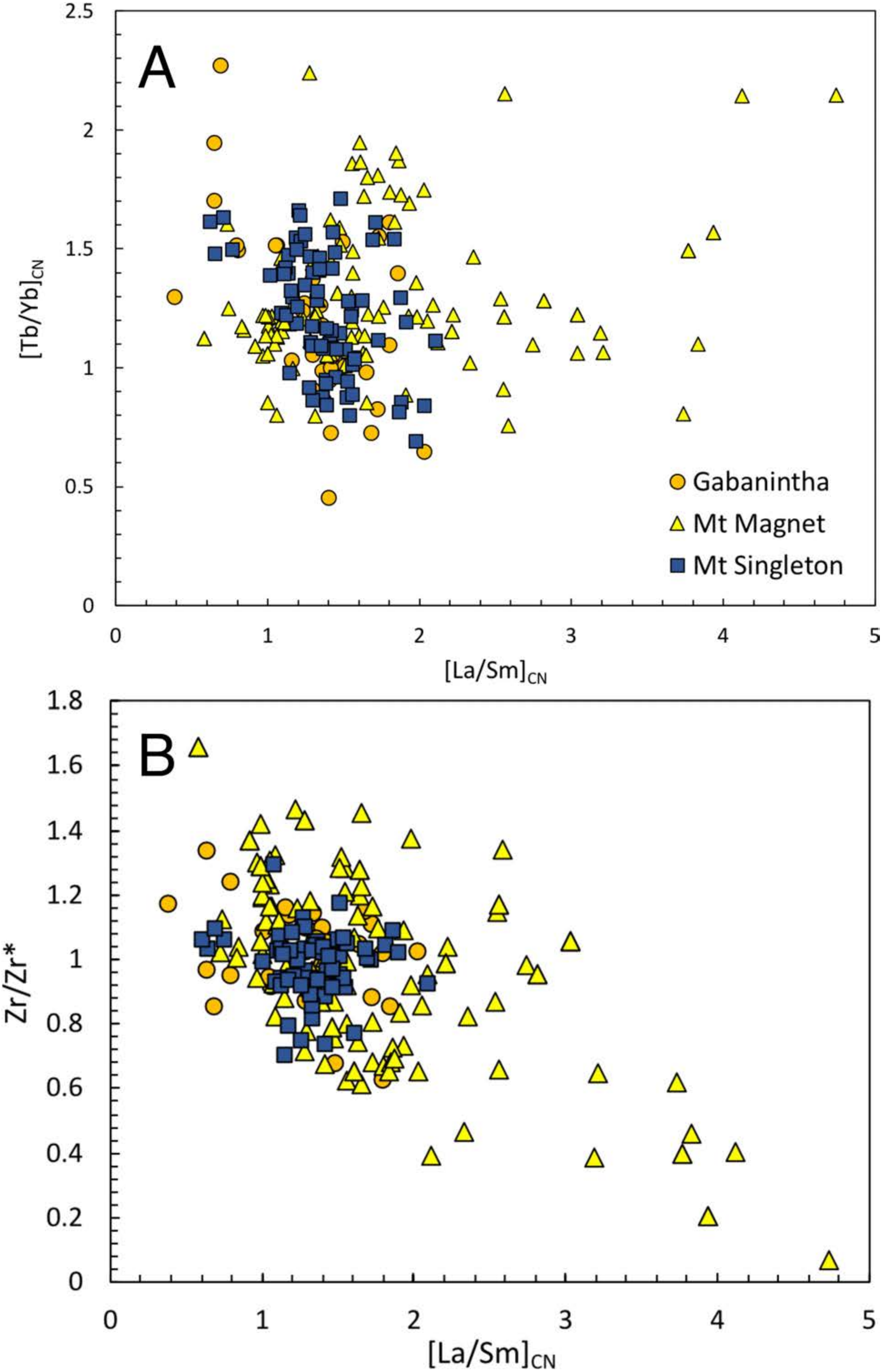
A
2.5
2
1.5
1
0.5
0
[Tb/Yb]CN
0
1
2
3
4
5
[La/Sm]CN
Gabanintha
Mt Magnet
Mt Singleton
B
1.8
1.6
1.4
1.2
1
0.8
0.6
0.4
0.2
0
Zr/Zr*
0
1
2
3
4
5
[La/Sm]CN

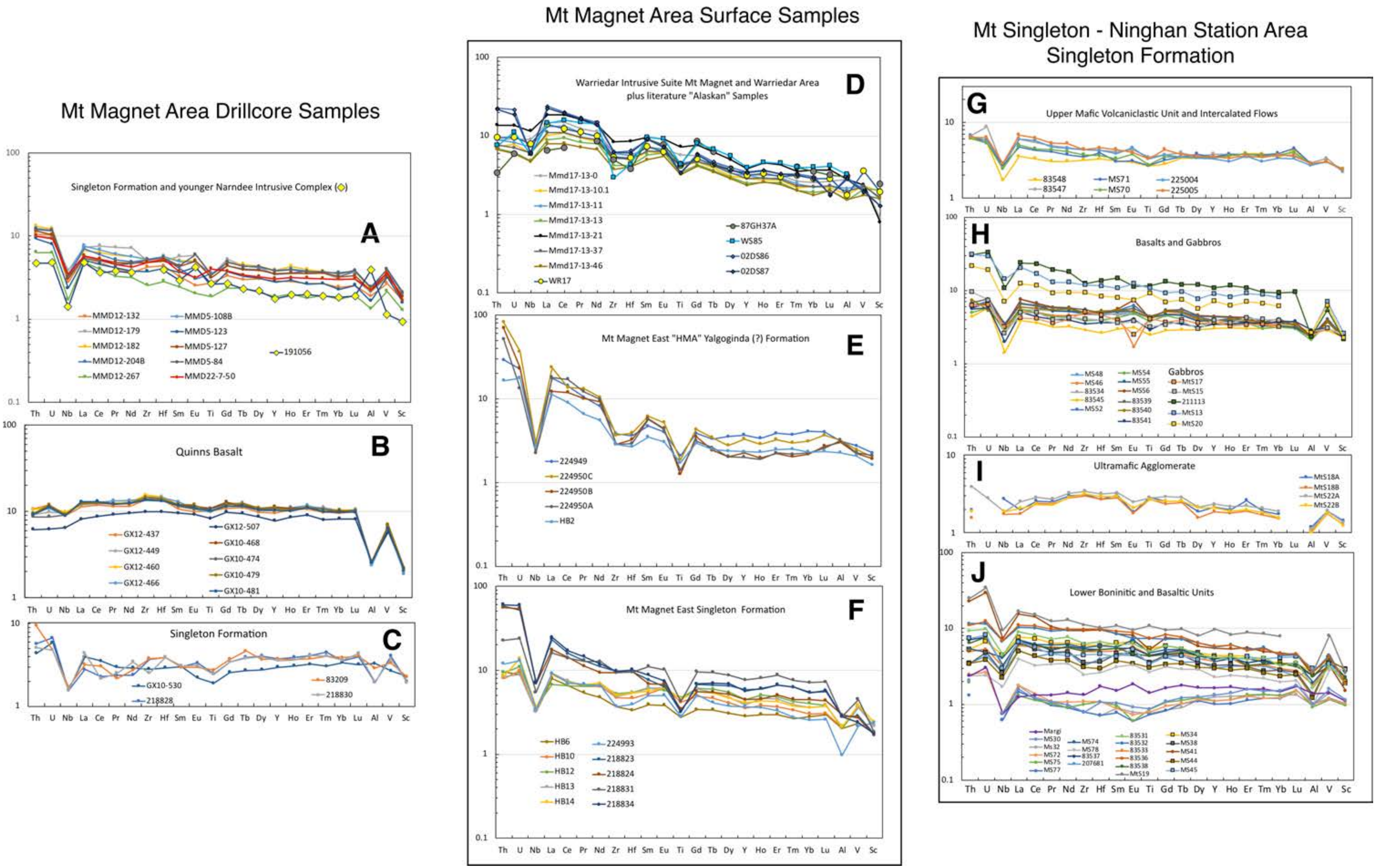

Mt Magnet Area Drillcore Samples
Mt Magnet Area Surface Samples
Mt Singleton - Ninghan Station Area
Singleton Formation
A
Singleton Formation and younger Narndee Intrusive Complex
MMD12-132
MMD12-179
MMD12-182
MMD12-204B
MMD12-267
MMD5-108B
MMD5-123
MMD5-127
MMD5-84
MMD22-7-50
191056
B
Quinns Basalt
GX12-437
GX12-449
GX12-460
GX12-466
GX12-507
GX10-468
GX10-474
GX10-479
GX10-481
C
Singleton Formation
GX10-530
218828
83209
218830
D
Warriedar Intrusive Suite Mt Magnet and Warriedar Area
plus literature "Alaskan" Samples
Mmd17-13-0
Mmd17-13-10.1
Mmd17-13-11
Mmd17-13-13
Mmd17-13-21
Mmd17-13-37
Mmd17-13-46
WR17
87GH37A
WS85
02DS86
02DS87
E
Mt Magnet East "HMA" Yalgoginda (?) Formation
224949
224950C
224950B
224950A
HB2
F
Mt Magnet East Singleton Formation
HB6
HB10
HB12
HB13
HB14
224993
218823
218824
218831
218834
G
Upper Mafic Volcaniclastic Unit and Intercalated Flows
83548
83547
MS71
MS70
225004
225005
H
Basalts and Gabbros
MS48
MS46
83534
83545
MS52
MS54
MS55
MS56
83539
83540
83541
Gabbros
MtS17
MtS15
211113
MtS13
MtS20
I
Ultramafic Agglomerate
MtS18A
MtS18B
MtS22A
MtS22B
J
Lower Boninitic and Basaltic Units
Margi
MS30
Ms32
MS72
MS75
MS77
MS74
MS78
83537
207681
83531
83532
83533
83536
83538
MtS19
MS34
MS38
MS41
MS44
MS45
Th U Nb La Ce Pr Nd Zr Hf Sm Eu Ti Gd Tb Dy Y Ho Er Tm Yb Lu Al V Sc

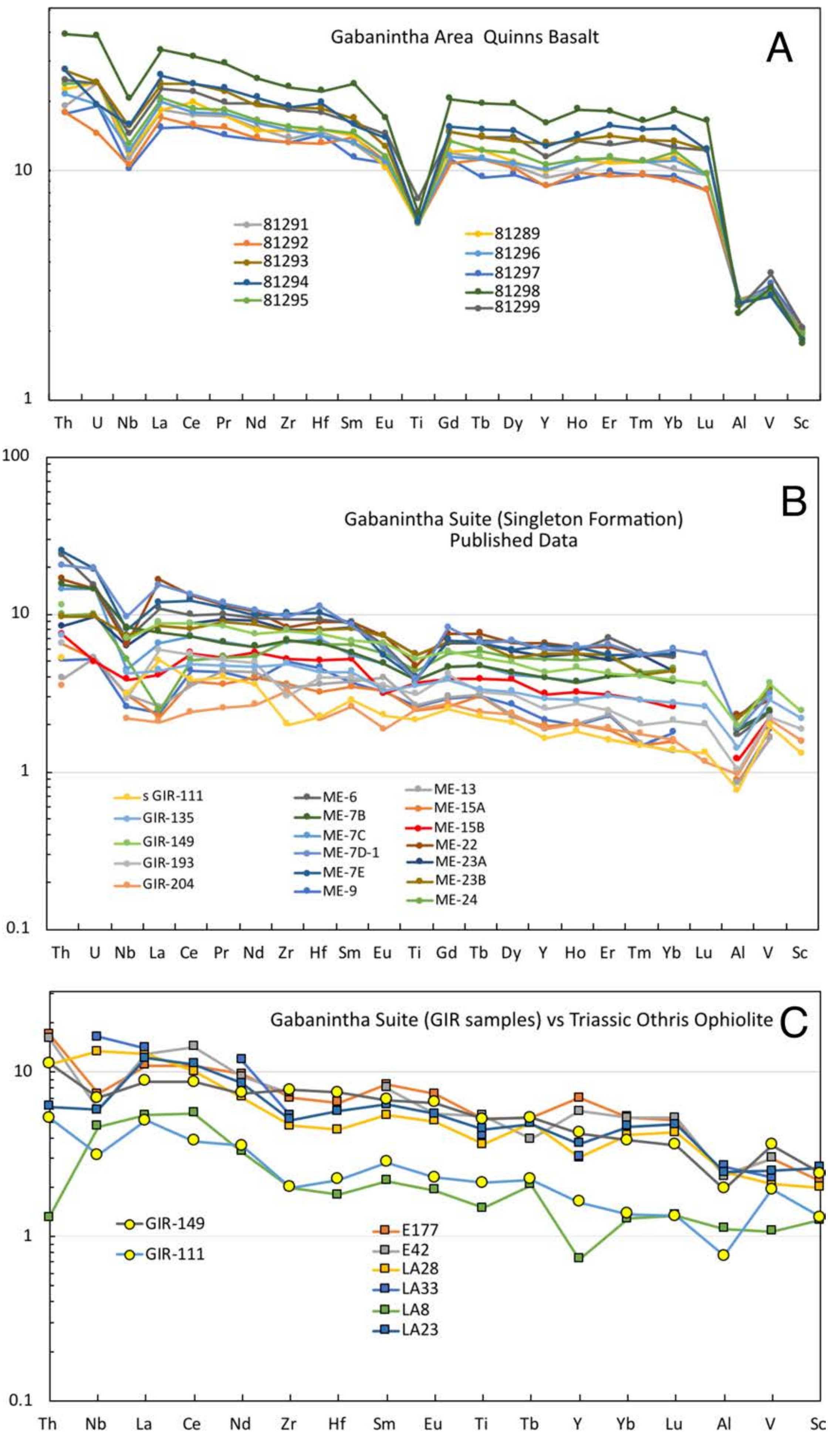
Gabanintha Area Quinns Basalt
A
10
1
81291
81292
81293
81294
81295
81289
81296
81297
81298
81299
Th U Nb La Ce Pr Nd Zr Hf Sm Eu Ti Gd Tb Dy Y Ho Er Tm Yb Lu Al V Sc
100
Gabanintha Suite (Singleton Formation)
Published Data
B
10
1
0.1
s GIR-111
GIR-135
GIR-149
GIR-193
GIR-204
ME-6
ME-7B
ME-7C
ME-7D-1
ME-7E
ME-9
ME-13
ME-15A
ME-15B
ME-22
ME-23A
ME-23B
ME-24
Th U Nb La Ce Pr Nd Zr Hf Sm Eu Ti Gd Tb Dy Y Ho Er Tm Yb Lu Al V Sc
Gabanintha Suite (GIR samples) vs Triassic Othris Ophiolite
C
10
1
0.1
GIR-149
GIR-111
E177
E42
LA28
LA33
LA8
LA23
Th Nb La Ce Nd Zr Hf Sm Eu Ti Tb Y Yb Lu Al V Sc

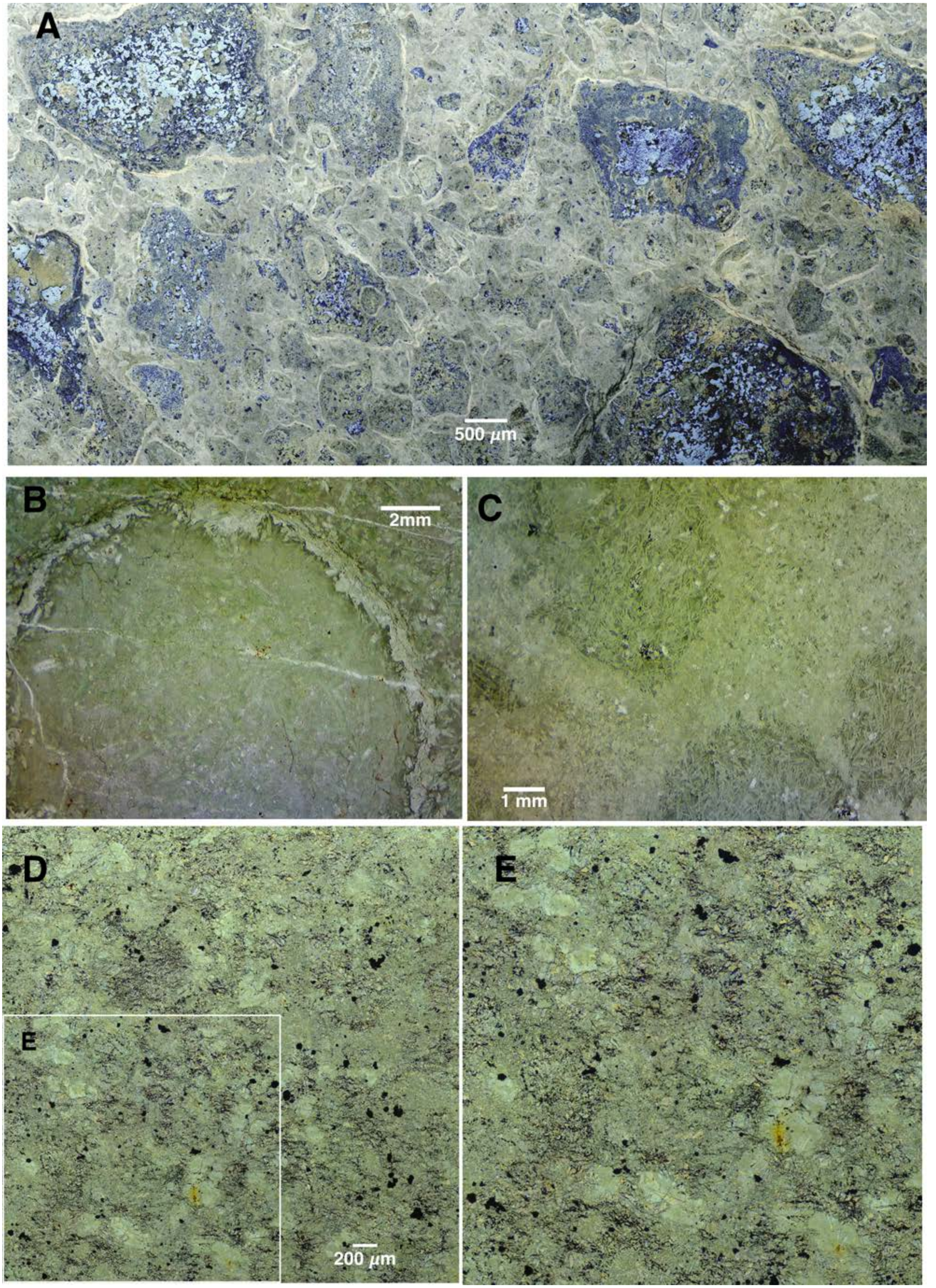
A
500 μm
B
2mm
C
1 mm
D
E
200 μm
E

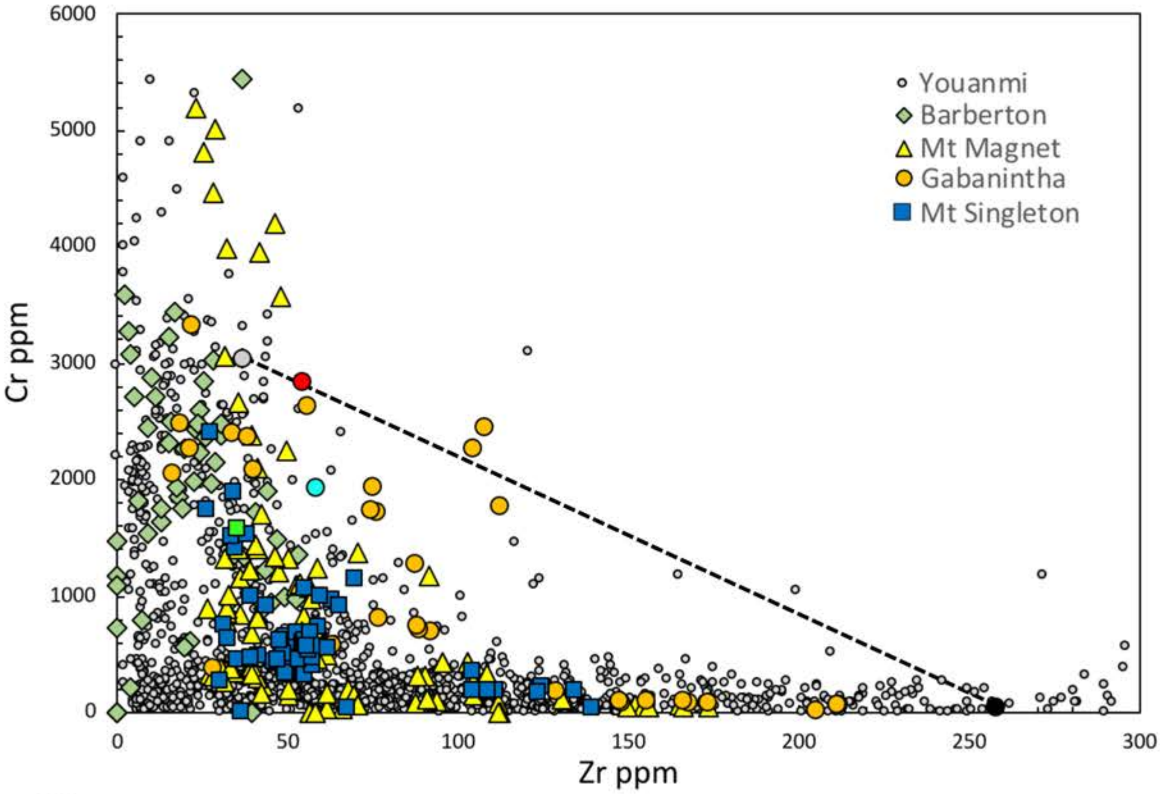

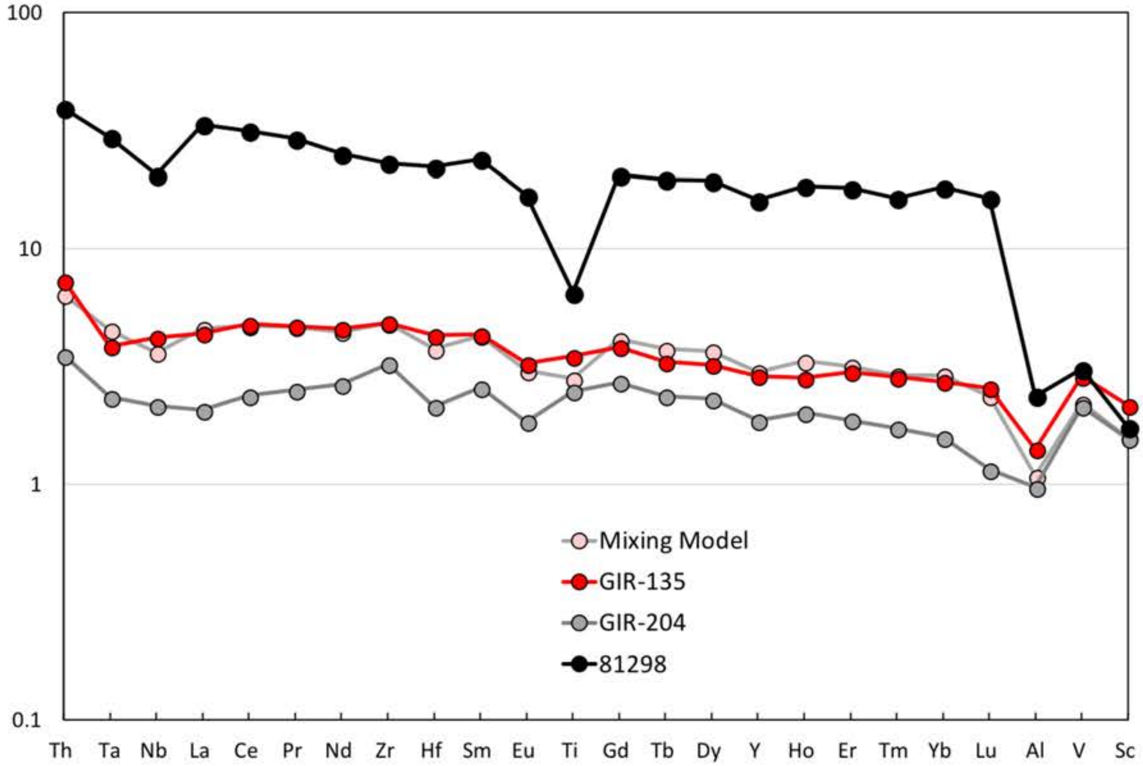

GIR-135 versus 0.92 Sample GIR-204 + 0.08 Sample 81928

ppm	Ti	Cr	Co	Ni
Mixture	3860	2810	84	1522
GIR-135	4804	2837	92	1312

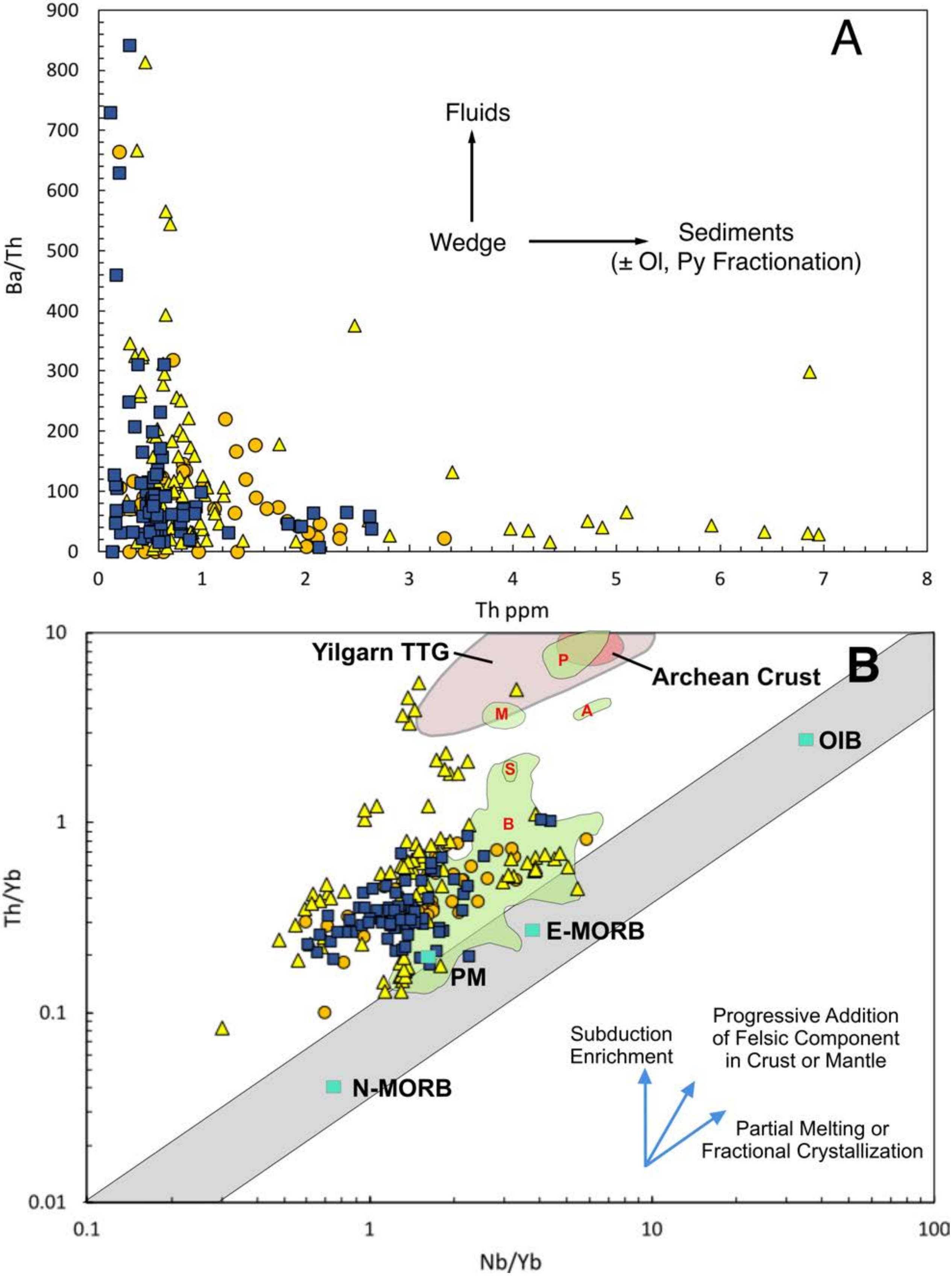

A
Ba/Th
Th ppm
Fluids
Wedge
Sediments
(± Ol, Py Fractionation)
B
Th/Yb
Nb/Yb
Yilgarn TTG
Archean Crust
P
M
A
S
B
OIB
E-MORB
PM
N-MORB
Subduction Enrichment
Progressive Addition of Felsic Component in Crust or Mantle
Partial Melting or Fractional Crystallization

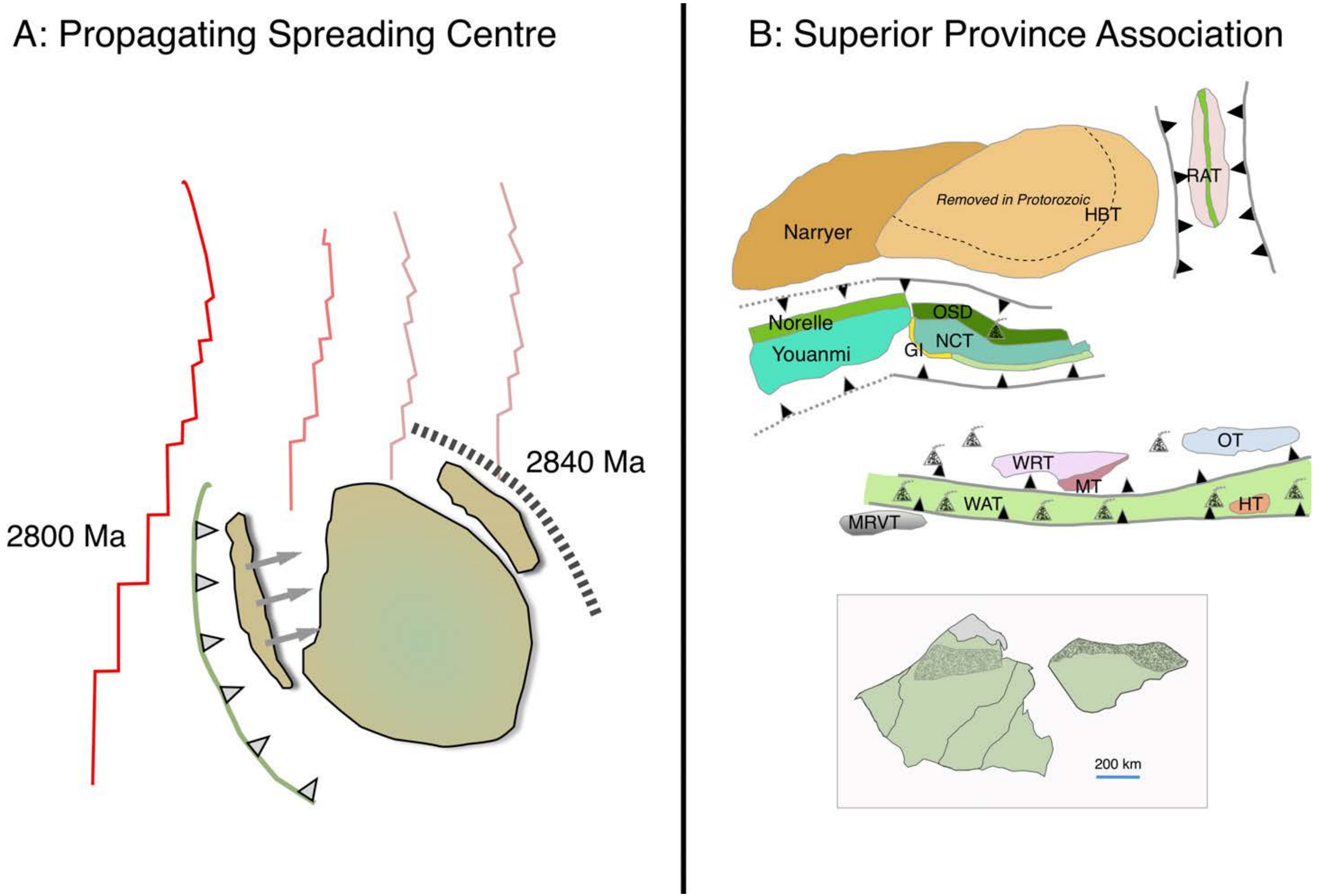
A: Propagating Spreading Centre
2840 Ma
2800 Ma
B: Superior Province Association
Removed in Protorozoic
HBT
Narryer
RAT
Norelle
OSD
NCT
Youanmi
GI
OT
WRT
MT
WAT
HT
MRVT
200 km